Characterization of Plasma Labile Heme in Hemolytic Conditions

Zélia Gouveia[1,#] Ana Rita Carlos[1], Xiaojing Yuan[2], Frederico Aires-da-Silva[3,4], Roland Stocker[5], Ghassan J. Maghzal[5], Sónia S. Leal[6], Cláudio M. Gomes[6,§], Smilja Todorovic[6], Olga Iranzo[6,£], Susana Ramos[1], Ana Catarina Santos[7,8], Iqbal Hamza[2], João Gonçalves[7,8] & Miguel P. Soares[1,*]

[1]Instituto Gulbenkian da Ciência, 2780-156 Oeiras, Portugal. [2]Department of Animal and Avian Sciences and Department of Cell Biology and Molecular Genetics, University of Maryland, College Park MD 20742, USA. [3]Technophage S.A. 1600-190 Lisboa, Portugal. [4]CIISA-Faculdade de Medicina Veterinária, Universidade de Lisboa, 1300-477 Lisboa, Portugal. [5]Vascular Biology Division, Victor Chang Cardiac Research Institute, Darlinghurst NSW 2010 Australia; University of New South Wales, NSW, Australia. [6]Instituto de Tecnologia Química e Biológica António Xavier, Universidade Nova de Lisboa, 2780-157 Oeiras, Portugal. [7]IMM, Faculdade. Medicina, Universidade de Lisboa, 1649-028 Lisboa, Portugal. [8]CPM-URIA Faculdade Farmácia, Universidade de Lisboa, 1649-003 Lisboa, Portugal. [#]Current address is Institute Curie, UMR144, 75000 Paris, France. [§]Current address is Faculdade de Ciências Universidade de Lisboa, Biosystems and Integrative Sciences Institute and Department of Chemistry and Biochemistry, Universidade de Lisboa, Portugal. [£]Current address is Aix Marseille Université, Centrale Marseille, CNRS, iSm2 UMR 7313, 13397 Marseille, France.

Correspondence to Miguel P. Soares; Instituto Gulbenkian de Ciência, Rua da Quinta Grande, 6, 2780-156 Oeiras, Portugal, Tel.: +351-214464520; E-mail: mpsoares@igc.gulbenkian.pt

Article type : Regular Paper

This article has been accepted for publication and undergone full peer review but has not been through the copyediting, typesetting, pagination and proofreading process, which may lead to differences between this version and the Version of Record. Please cite this article as doi: 10.1111/febs.14192

Running Title: ***Labile heme***

Abbreviations: ATR, Attenuated total reflectance; β-ME, β-mercaptoethanol; BV, Biliverdin; BR, bilirubin; biotin, N-[-5-(Hydrazinocarboxy) pentyl]-D-biotinamide; CCD, charge coupled device; CD, Circular Dichroism; CDR, complementary determining region; CN, cysteine-asparagine; CoPP, cobalt PP; CS, cysteine-serine; Cytc, cytochrome c; DeuP, deuteroporphyrin IX; DHB, dihydroxybenzoic acid; Fe, iron; FePP, heme; GaPP, gallium protoporphyrin IX; HA, hemagglutinin; HABA, 4'-hydroxyazobenzene-2-carboxylic acid; HBM, heme binding motifs; Hb, hemoglobin; HBC, heme binding capacity; HPX, hemopexin; HPLC, high performance liquid chromatography; HRP, horseradish peroxidase; HSA, Human serum albumin; FTIR, Fourier transform infrared;; iRBC, infected RBC; LB, Luria broth; mAb, monoclonal antibody; MetHb, oxidized Hb; Mb, myoglobin; NO, oxide; pNPP, para-Nitrophenylphosphate; PBS, Dulbecco's Phosphate Buffered Saline; PP, protoporphyrin; SA, succinylacetone; SdAb, single-domain antibody; SDS-PAGE, Sodium dodecyl sulfate-polyacrylamide gel electrophoresis; SnPP, TOFMS, (MALDI)-Time-of-flight mass spectrometry; TinPP; TNF, tumor necrosis factor; RBC, red blood cell; RR, Resonance Raman;; ZnPP, Zinc protoporphyrin

Keywords: hemolysis, hemoglobin, heme, malaria, sickle cell disease, antibody engineering, single-domain antibody.

Conflicts of interest: The authors declare no competing financial interests.

ABSTRACT

Extracellular hemoglobin (Hb), a byproduct of hemolysis, can release its prosthetic heme groups upon oxidation. This produces metabolically active heme that is exchangeable between acceptor proteins, macromolecules and low molecular weight ligands, termed here labile heme. As it accumulates in

plasma labile heme acts in a pro-oxidant manner and regulates cellular metabolism while exerting pro-inflammatory and cytotoxic effects that foster the pathogenesis of hemolytic diseases. Here we developed and characterized a panel of heme-specific single domain antibodies (sdAbs) that together with a cellular-based heme reporter assay, allow for quantification and characterization of labile heme in plasma during hemolytic conditions. Using these approaches we demonstrate that labile heme generated during hemolytic conditions is bound to plasma molecules with an affinity higher than 10^{-7} M and that 2-8% (~2-5 μM) of the total amount of heme detected in plasma can be internalized by bystander cells, *i.e*. bioavailable heme. Acute, but not chronic, hemolysis is associated with transient reduction of plasma heme binding capacity ($HBC_{1/2}$), that is, the ability of plasma molecules to bind labile heme with an affinity higher than 10^{-7}M. The heme-specific sdAbs neutralize the pro-oxidant activity of soluble heme *in vitro*, suggesting that these maybe used to counter the pathologic effects of labile heme during hemolytic conditions. Finally, we show that heme-specific sdAbs can be used to visualize cellular heme. In conclusion, we describe a panel of heme-specific sdAbs that when used with other approaches provide novel insights to the pathophysiology of heme.

INTRODUCTION

Heme consists of a tetrapyrrole ring bound to iron (Fe) *via* several nitrogens. Heme exists essentially as a prosthetic group of hemoproteins [1], including hemoglobin (Hb) [2], where Fe binds to the gaseous molecules oxygen (O_2), nitric oxide (NO) [3] or carbon monoxide (CO) [4] *via* effective back-donation of Fe $d\pi_x$ electrons to low-lying π^* orbitals of these diatomic molecules. Heme displays subtle chemical modifications, giving rise to the different types, mainly the *a*, *b* and *c* variants [5]. The most common and abundant heme type in mammals is heme *b* present in Hb and myoglobin, among other hemoprotein. Whereas heme *c* can bind covalently to proteins *via* two thioester bonds, heme *b* and *a* cannot and are released from hemoproteins, such as observed upon Hb oxidation [6-9]. While often referred as "free heme" [10, 11], the heme released from hemoproteins is most probably never in "free form". Labile heme is the term used to refer to the pool of metabolically active heme, which is loosely bound to acceptor proteins, therefore becoming exchangeable with other macromolecules and low molecular weight ligands [12]. Of note, while heme is a stable molecule, the

term “labile” is used to emphasis that “labile heme” is more readily prone to alteration of its redox state, imposed by its immediate environment.

In adult humans, the sheer number of red blood cells (RBC; ~2-3x10^{13}) coupled to their high Hb (~3x10^{8} molecules/RBC) and heme (~1.2x10^{9} molecules/RBC)[13] content create a situation in which clinically silent levels of intravascular hemolysis can be associated with the release of relatively high amounts of Hb into plasma. Upon oxidation, extracellular Hb can release its non-covalently bound heme groups [6-9], generating pro-oxidant labile heme [8, 14, 15] that acts as a alarmin [16], sensed by pattern recognition receptors, such as Toll like receptor 4 (TLR4)[17] or NACHT, LRR and PYD domains-containing protein 3 (NALP3) [18]. This endows labile heme with pro-inflammatory [16-20], vasoactive [21] and cytotoxic [10, 22-25] effects, while also regulating metabolism [26] and interfering with coagulation [27]. Presumably these pathophysiologic effects of labile heme contribute critically to the pathogenesis of hemolytic conditions, such as malaria caused upon infection by the protozoan parasites of the genus *Plasmodium* [6, 28], severe sepsis caused by polymicrobial infections [10] or sickle cell disease caused by mutations in the gene encoding the β chain of Hb [21, 29, 30].

Current limitations in methodologies allowing for accurate quantification of labile heme or providing further information on its biological environment make it particularly challenging to ascertain the contribution of labile heme to the pathogenesis of hemolytic conditions. Here we developed a panel of heme-specific single domain antibodies (sdAb) that, when used together with other approaches [31], allow to quantify and characterize labile heme in plasma, its rate of cellular internalization and cellular localization. We report that intravascular hemolysis in mice is associated with the accumulation of labile heme in plasma, which is bound to plasma molecules with an affinity higher than 10^{-7} M. We estimate that about 2-8% (~2-5 μM) of the heme released in plasma during hemolytic conditions becomes “bioavailable”, being internalized by bystander cells. Heme-specific sdAb can be used to neutralize the pro-oxidant effect of labile heme in solution, an effect that could have therapeutic implications in the treatment of infectious as well as non-infectious hemolytic conditions. Finally, we demonstrate that heme-specific sdAb can be used to monitor intracellular heme, detected primarily in the mitochondria.

RESULTS

Generation of heme-specific SdAbs

We screened a synthetic phage-display sdAb library [32], derived from a highly soluble and stable VL scaffold [33] against heme *b*, biotinylated in a single carboxylic group, corresponding to a molecular weight of 969.2 Da (Fig. 1A,B). Phages encoding sdAb recognizing biotinylated heme were selected using streptavidin-magnetic beads (Fig. 1C,D), essentially as described [34]. An ELISA, using non-biotinylated heme as a solid phase antigen, was used to determine the relative heme-binding capacity of the selected sdAb. Relative heme recognition was normalized to the relative amount of sdAb, as detected by ELISA, using a monoclonal antibody (mAb) against the human influenza hemagglutinin (HA) epitope expressed in the C-terminus of these sdAb. Eleven sdAbs were selected through this assay (Fig. 1E), expressed in *E. coli* BL21 and purified under denaturing conditions before refolding by step-wise dialysis [35]. Protein yield was typically around 10 mg/L with >90% purity, as assessed by SDS-PAGE (Fig. 1E). Expression of the ~15 kDa protein corresponding to the full-length sdAb containing the MKKTAIAIAVALAGFATV leader peptide sequence and a ~13kDa protein corresponding to the leaderless sdAb, was confirmed by western blot (Fig. 1E).

We then compared the relative capacity of the purified sdAbs used at the same concentration to bind a solid-phase heme in an ELISA (Fig. 1F). The affinity (K_D) of these sdAb towards heme was determine by surface plasmon resonance and estimated to be in the order of 10^{-7} M, with the exception of sdAb 1E4, which has an affinity of 10^{-5}M towards heme (Fig. 1G). Further *in silico* analyses revealed that the complementarity-determining region (CDR) 1 of all the selected sdAbs carries potential heme binding motifs [36], including cysteine-X-X-cysteine-Lysine (CXXCK; were X is any amino acid (aa)) characteristic of hemoproteins that bind heme *c* [37], CK*, i.e.* sdAb 1A6, CN, *i.e.* sdAb 2H7 or CS, *i.e.* sdAb 2H10, 1G3, 2A12, 1C2 and 2H5, characteristic of hemoproteins that bind heme *b* (Fig. 1G). Based on their heme affinity and the presence of putative heme binding motifs we selected the sdAbs 1A6, 2H7 and 2H10 for further analyzes. Of note, CDR3 sequences where absent in these sdAbs.

SdAbs specificity

To determine the relative specificity of sdAbs 1A6, 2H7 and 2H10, these were pre-incubated with a variety of heme-related molecules and their capacity to bind solid-phase bound heme was assessed by ELISA. Heme (FePP) was used a positive control, gallium protoporphyrin (PP) IX (GaPP) as a non-Fe metallated porphyrin containing redox inert gallium instead of Fe and PP IX (PP) as metal-free precursor of heme. As expected, pre-incubation with FePP abolished subsequent recognition of solid-phase bound heme by all three sdAbs (Fig. 2A). Pre-incubation with PP inhibited heme recognition by sdAb 1A6 but not by sdAbs 2H7 and 2H10 (Fig. 2A). This suggests that Fe, present in FePP but not in PP, is required for heme recognition by sdAbs 2H7 and 2H10 but not by the sdAb 1A6. Pre-incubation with GaPP abolished heme recognition by all three sdAbs (Fig. 2A). Given that gallium is not readily reduced, mimicking Fe^{3+}, this observation suggests that all three sdAbs recognize preferentially oxidized Fe^{3+}PP, consistent with their initial selection under aerobic conditions favoring heme oxidation into Fe^{3+}PP. To assess the relative contribution of the porphyrin side chains to heme recognition, the sdAb were pre-incubated with Fe deuteroporphyrin IX (DeutP), a synthetic heme derivative lacking the heme vinyl group or with FePP IX dimethyl ester chloride (FePPCH3) in which the two-propionate side chains are methylated (Fig. 2B). While DeutP inhibited heme recognition by all three sdAb (Fig. 2B), FePPCH3 inhibited heme recognition by sdAb 1A6 and 2H7 but only to a lesser extent by sdAb 2H10. This suggests that heme recognition by sdAb 2H10 involves a carboxylic acid in the propionate side chains (Fig. 2B).

Pre-incubation with biliverdin or bilirubin, a direct and an indirect end product of heme catabolism, respectively, partially inhibited heme recognition by sdAb 1A6 but not by sdAb 2H10 (Fig. 2C). Recognition of solid-phase bound heme by the sdAb 2H7 was partially inhibited by biliverdin but not by bilirubin (Fig. 2C). This suggests that the sdAb 2H10 is probably the only one, among these three sdAbs, that recognizes specifically heme. This is consistent with the preferred V-shaped ridge tile conformation of bilirubin [38], being quite distinct from heme and as such unlikely to be recognized by the same linear aa motif used to recognize heme in 2H10 sdAb.

We then asked whether these sdAbs recognize porphyrins containing divalent metals, other than Fe, such as tin PP (SnPP), cobalt PP (CoPP) or Zinc PP (ZnPP). Pre-incubation of sdAbs 1A6, 2H7

and 2H10 with SnPP or CoPP inhibited their binding to solid-phase bound heme (Fig. 3A), while pre-incubation with ZnPP inhibited heme recognition by sdAb 2H7 but not by sdAb 1A6 and 2H10 (Fig. 3A). This suggests that the chemical properties of the metal at the center of the protoporphyrin ring may be important for heme recognition by sdAb 1A6 and 2H10 but not by sdAb 2H7.

We also asked whether these sdAbs recognized Fe in the absence of a porphyrin ring. Pre-incubation with $Fe_2(SO_4)_3$ failed to inhibit the recognition of solid-phase-bound heme by all three sdAbs (Fig. 3B), suggesting that Fe *per se* is not required for heme recognition by these sdAb. Finally, we asked whether these sdAbs recognize heme contained inside hemoproteins. Pre-incubation of the sdAbs with Hb, oxidized Hb (MetHb), myoglobin (Mb), albumin bound to heme *b* or cytochrome c failed to inhibit the recognition of solid-phase bound heme by all three sdAbs (Fig. 3C). This suggests that while these sdAbs recognize soluble heme they fail to recognize heme when it is incorporate in hemoproteins. Table 1 summarizes these results.

Structural characterization of sdAbs-heme complexes

We used a heme-biotin pull-down assay to compare the relative capacity of sdAbs 1A6, 2H7 and 2H10 to recognize heme in solution. All three sdAbs bound heme-biotin in solution, with 1A6 and 2H10 showing higher binding capacity, as compared to 2H7 (Fig. 4A), consistent with their relative affinity towards heme (Fig. 1G).

We used UV-visible spectroscopy to monitor heme (Fig. 4B) and heme binding to sdAbs (Fig. 4C). The UV-visible spectrum of heme (Fig. 4B) shows two overlapping bands, at ~ 363 and 383 nm, in the Soret region and a charge transfer band at 622 nm, indicating high spin Fe^{3+} state. The UV-visible spectrum of sdAb bound to heme shows a δ band at 360 nm, an intense Soret band at 412 nm, two weak Q bands at 530 and 565 nm and another 624 nm band in the charge transfer region (Fig. 4C). The Soret band indicates the presence of Fe^{3+}, the 530 and 565 nm bands are consistent with the presence of a six-coordinated low spin Fe^{3+} state, the δ band at 360 nm suggests the presence of a thiol axial heme ligation [39] and the 624 nm band is indicative of either Cys or porphyrin to high spin Fe^{3+} charge transfer (Fig. 4C). With the exception of the charge transfer band, UV-visible features of the

sdAb/heme complex are similar to the spectra of ferric cytochrome P450cam, carrying Cys and H_2O axial ligands [40].

Heme binding was associated with alterations in the secondary structure of the sdAb, as assessed by circular dichroism (CD) and Attenuated total reflection Fourier Transform infrared (ATR-FTIR) spectroscopies for sdAb 2H10. Namely, the far-UV CD spectrum revealed a negative band centered at 218 nm, indicative of a β-sheet protein fold (Fig. 4D). Heme binding resulted in broadening of this band, suggesting a conformational rearrangement of secondary structure elements (Fig. 4D). Analysis of the Soret region reflects heme coordination with the appearance of a positive CD band at 412 nm, absent in apo-2H10 sdAb (Fig. 4D, inset).

The impact of heme coordination on the secondary structure of sdAb 2H10 was further analyzed by ATR-FTIR, which is sensitive to different types of β-sheet structures. A comparison of the absorption spectra of sdAb 2H10 in the presence/absence of heme, in the amide I region (1700-1610 cm^{-1}) is indicative of structural alterations upon heme coordination (Fig. 4E**,** top). Second derivative analysis of the ATR-FTIR spectra, performed to identify individual components under the intrinsically broad amide I band envelope [41], revealed major contributions typical of β-sheet structures for apo-2H10, in agreement with CD data (Fig. 4E*,* bottom). The presence of 1633 and 1693 cm^{-1} bands simultaneously is most likely associated with an anti-parallel arrangement of β-strands in sdAb 2H10, which are typically characterized by a strong band at ~1630 cm^{-1} and a weaker one at ~1690 cm^{-1}. Upon heme ligation, there was a rearrangement in β structures with the β-turn band at 1668 cm^{-1} shifting to 1678 cm^{-1} and a lack of the contribution at 1693 cm^{-1}, which denotes a loss of the anti-parallel β-sheet fingerprint. Thus, the sdAb 2H10 is likely composed of anti-parallel β-sheets, which undergo conformational changes upon heme binding.

Resonance Raman (RR) spectroscopy was used to further characterize the heme moiety in the sdAb heme-2H10 complex. Upon excitation into the Soret electronic transition band, RR spectra display in the high frequency region (1300-1700cm^{-1}) core size marker bands (*e.g.* ν_4, ν_3, ν_2 and ν_{10}), which are sensitive to coordination, spin and redox state of the heme Fe. A comparison of RR spectra of hemin versus the sdAb-heme complex (Fig. 4F) demonstrates that the sdAb 2H10 binds in a specific manner to heme *b*, revealed by changes in frequency and relative intensity of spin state

sensitive ν_3, ν_2 and ν_{10} modes. Also, the bandwidth of the well-defined ν_3 mode revealed one spin species (*i.e.* one type of ligation) in the complex. The ν_4 at 1377 and 1373 cm^{-1} in the heme-2H10 complex and heme, respectively, indicate in both cases a Fe^{3+} state of the heme-Fe. The heme-2H10 complex revealed the ν_3 and ν_2 at 1508 and 1585 cm^{-1} respectively, characteristic for six-coordinated low spin heme Fe (Fig. 4F). These modes were found at 1492 and 1571 cm^{-1}, respectively in the heme spectra, indicating a five-coordinated high spin (Fig. 4F) state, with most likely a Cl^- ion acting as the fifth axial ligand. The most probable candidates for heme axial ligands in the six-coordinated low spin 2H10-heme complex are tyrosine (Y) and lysine (K), besides cysteine (C), as established by the UV-Vis spectra. These aa are present in the CDR1 of sdAb 2H10 (Fig. 1G) as well as axial ligands in several hemoproteins [36]. Also, the H_2O molecule, which in some heme proteins acts as a strong axial ligand, cannot be excluded.

We then analyzed the effect of pH on sdAb binding to heme. Heme binding by sdAb 2H10 was inhibited at pH 4.0-4.5 (Fig. 5A). Restoring pH to 7.0 reestablished heme recognition by sdAb 2H10, despite some level of sdAb precipitation (Fig. 5B). We also addressed whether Ca^{2+} or Mg^{2+} interfere with heme binding by this sdAb. We found that heme-binding to sdAb 2H10 was impaired by Ca^{2+} but not by Mg^{2+} (Fig. 5C,D). This suggest that while divalent metals, such as Fe^{2+} or Mg^{2+}, do not appear to interfere with sdAb binding to heme, Ca^{2+} can modulate heme binding to the sdAb 2H10.

Characterization of labile heme in plasma during hemolytic conditions

Induction of acute hemolysis in C57BL/6 mice, by the administration of phenylhydrazine, was associated with a marked reduction of circulating RBC numbers (Fig. 6A) and increased heme concentration in plasma (Fig. 6B), *i.e.* from 23,4 ± 7,1 µM at steady state [29] to 120,8 ± 26,6 µM, 24 hours after phenylhydrazine administration (Fig. 6B). There was negative correlation between the number of circulating RBC and the concentration of heme in plasma, that is, lower numbers of circulating RBC were associated with higher concentration of heme in plasma (Fig. 6C).

Heme accumulation in plasma, 24 hours after phenylhydrazine administration, was associated with heme uptake by bystander cells, *i.e.* 4.8 ± 0.6 µM (Fig. 6D), as assessed *in vitro* using a cellular heme reporter assay [12, 31]. Briefly, HEK293 cells transiently transfected with horseradish peroxidase

based reporter were exposed to mouse plasma, containing an unknown amount of heme that that can be internalized, as reveled by the acquisition of intracellular HRP activity. By comparison with a standard curve of soluble heme one can infer on the amount of bioavailable heme in plasma and estimate it to correspond to about 4% of the total amount of heme detected in the plasma of these mice (Fig. 6D). There was a negative correlation between the number of circulating RBC and the concentration of bioavailable heme in plasma, that is, the lower the number of circulating RBC the higher the concentration of bioavailable heme in plasma (Fig. 6E).

We developed a sandwich ELISA to quantify heme in solution, using solid-phase bound sdAb 1A6 to capture soluble heme and biotinylated 2H7 sdAb to detect heme bound to the sdAb 1A6. The assay quantifies heme in solution, in a linear range from 0.15 to 2.5 μM(Fig. 6F). Using this sdAb-based ELISA we did not detect heme in the plasma of C57BL/6 mice subjected phenylhydrazine administration (data not shown). However, considering that the heme-specific sdAbs have an affinity of 10^{-7} M towards heme (Fig. 1G), the ELISA should detect only heme not bound to other molecule with an affinity higher than 10^{-7} M. This suggests therefore that the bioavailable heme detected in the plasma of C57BL/6 mice receiving phenylhydrazine is bound to plasma molecules with an affinity higher than 10^{-7} M. In keeping with this notion, the same ELISA also did not recognize heme bound to HPX (Fig. 6G).

We then asked whether plasma proteins with high affinity towards heme, such as HPX, can uptake heme bound to the heme-specific sdAb. We confirmed that HPX can take-up heme from the sdAb 2H10, using an *in vitro* pull-down assay with streptavidin-beads capturing biotinylated-heme bound to sdAb 2H10, in the presence or absence of HPX (Fig. 6H). Namely when apo-HPX is added to the sdAb 2H10 bound to biotinylated-heme, the streptavidin-beads pull-down both the sdAb 2H10 and the HPX, revealing that HPX removed the biotinylated-heme from the sdAb 2H10 (Fig. 6H).

We adapted the heme-specific ELISA to quantify the relative capacity of plasma macromolecules or other low molecular ligands to bind heme with an affinity higher than 10^{-7} M, that is, the plasma heme binding capacity ($HBC_{1/2}$). Briefly, Plasma is incubated in vitro with increasing concentrations of heme, until saturation of heme-binding molecules with an affinity towards heme higher than 10^{-7} M. The heme-specific sdAb-based ELISA is used, as described above, to detect excess heme and the

concentration of heme required to reduce by 50% the plasma HBC is defined as $HBC_{1/2}$. Induction of acute hemolysis reduced the $HBC_{1/2}$ of C57BL/6 mice, from 23.8±1.9 mM at steady state to 16.7±2.1 mM within 6 hours of phenylhydrazine administration, returning to steady state levels by 12 hours (Fig. 6I). This suggests that the majority of labile heme generated during acute hemolysis is readily bound by plasma molecules with an affinity $>10^{-7}$ M and cleared thereafter.

We then asked whether chronic hemolysis induced by *Plasmodium* infection is associated with the detection of labile heme in plasma. Infection of C57BL/6 mice with *Plasmodium chabaudi chabaudi* (*Pcc*) was associated with a progressive increase in the number of infected RBC until day 7, decreasing thereafter until day 9 post-infection (Fig. 7A). The peak of infection was associated with heme accumulation in plasma, i.e. 237,8±28,2 µM, decreasing thereafter to return to basal levels 9 days post-infection (Fig. 7B). There was a positive correlation between the percentage of infected RBC and the concentration of heme in plasma, with higher percentage of infected RBC associated with higher concentration of heme in plasma (Fig. 7C). *Plasmodium* infection was not associated with a reduction of plasma $HBC_{1/2}$ (Fig. 7D) and the levels of labile heme detected by the sdAb-based ELISA remained above 0.15 µM (*data not shown*). Nevertheless, 1-2% of heme detected in plasma at day 7 post infection, *i.e.* 3.9 ± 0.3 µM, became bioavailable, as assessed *in vitro* using a cellular heme reporter assay (Fig. 7E). There was a positive correlation between the percentage of infected RBC and the concentration of bioavailable heme in plasma (Fig. 7F). While this confirms that the blood stage of *Plasmodium* infection is associated with the accumulation high levels of heme in plasma [6, 10, 11, 22, 28, 42], labile heme is bound to plasma molecules with an affinity higher than 10^{-7} M, and therefore cannot be detected by the sdAb-based ELISA. A proportion of the labile heme that accumulates in plasma is bioavailable and therefore likely to participate in the pathogenesis of severe forms of malaria [6, 10, 11, 22, 28, 42].

We then asked whether the development of chronic hemolysis caused by the sickle Hb mutation, is associated with the accumulation of labile heme in plasma. We tested this hypothesis in knock-in C57BL/6;129 $h\alpha/h\alpha::\beta^S/\beta^S$ mice, a well-established experimental model of sickle-cell disease [43]. Heme concentration in the plasma of C57BL/6;129 $h\alpha/h\alpha::\beta^S/\beta^S$ knock-in mice was 27.0±3.9 µM, as compared to 18.5±3.9 µM and 19.9±3.4 µM in control C57BL/6;129 $h\alpha/h\alpha::\beta^A/\beta^S$ and $h\alpha/h\alpha::\beta^A/\beta^A$

mice that do not develop sickle cell disease, respectively (Fig. 8A). There was no apparent reduction of plasma $HBC_{1/2}$ in hα/hα::β^S/β^S mice, as compared to control hα/hα::β^A/β^S or hα/hα::β^A/β^A mice (Fig. 8B). Detection of labile heme, using the sdAb-based ELISA, remained above 0.15 µM (data not shown). Nevertheless, about 8% of the heme detected in the plasma of hα/hα::β^S/β^S mice became bioavailable, i.e. 2.1±0.9 µM, as assessed *in vitro* using a cellular heme reporter assay (Fig. 8C). This was not the case in control hα/hα::β^A/β^A or hα/hα::β^A/β^S mice (Fig. 8C). This confirms that sickle cell disease is associated with the accumulation of labile heme in plasma [21, 30, 44, 45] and supports the notion that labile heme promotes the pathogenesis of this hemolytic condition [21, 30, 44, 45].

Heme-specific sdAb modulate the redox activity of labile heme

We assessed whether heme binding by sdAb 2H10 interferes with the redox activity of labile heme, as assessed by electron exchange between heme and ascorbic acid in the presence of H_2O_2. Heme catalyzed ascorbic acid oxidation in a dose-dependent manner, that is, higher heme concentrations (0-5 µM) depleted ascorbate, as detected by HPLC (Fig. 9A, B). This pro-oxidant effect of heme was attenuated by sdAb 2H10, as compared to equimolar concentrations of control sdAb or human serum albumin (HSA) (Fig. 9A). Importantly, sdAb 2H10 also inhibited the pro-oxidant activity of heme/H_2O_2 in a concentration-dependent manner that is higher sdAb concentrations reduced ascorbate depletion (Fig. 9B). At each concentration tested, the sdAb 2H10 was more effective than the control sdAb or HSA in terms of preventing heme-driven ascorbate depletion (Fig. 9B).

Heme-specific SdAbs detect cellular heme

We asked whether heme-specific sdAbs can be used to detect intracellular heme by immunofluorescence and/or by flow cytometry. Intracellular heme was detected by immunofluorescence, in the perinuclear area of HeLa cells, using sdAb 1A6, 2H7 and 2H10, as compared to a control sdAb (Fig. 10A). Intracellular heme was also detected by flow cytometry using the same sdAbs (Fig. 10B). Detection of intracellular heme by the sdAb 2H10 was suppressed when the sdAb was pre-incubated with increasing heme concentrations, as assessed by flow cytometry (Fig.

10C) or by immunofluorescence (Fig. 10D). Pre-incubation of sdAb 2H10 with PP failed to inhibit intracellular heme detection by flow cytometry (Fig. 10E).

Having established that the heme-specific sdAbs can be used to detect intracellular heme, we addressed in more detail the intracellular localization of heme. Detection of intracellular heme by sdAb 2H10 overlapped with mitochondria staining by MitoTracker (Fig. 10F) and to a minor extent with endoplasmic reticulum (ER) staining by an anti-Calnexin monoclonal Ab (mAb) (Fig. 11A) or with early endosome staining by an anti-early endosome antigen 1 (EEA-1) staining (Fig. 11B), as detected by confocal microscopy. There was no overlap between heme and actin staining (Fig. 11C) and some minimal level of heme co-localization with heme oxygenase-1 (HO-1) (Fig. 11D) and bilirubin (Fig. 11E).

DISCUSSION

About 75-80% of bioavailable Fe in mammals is contained within the prosthetic heme groups of hemoproteins, with Hb containing the major pool of heme [25]. Extracellular Hb and heme are scavenged in plasma by haptoglobin and HPX, respectively [46]. Presumably accumulation of labile heme in plasma only takes place once the scavenging capacity of haptoglobin and HPX are saturated [10, 11, 16, 47, 48]. When this occurs, labile heme acts in a pro-oxidant [49, 50], pro-inflammatory [17, 51], vasoactive [21] and cytotoxic [10, 22, 23] manner that contributes to the pathogenesis of hemolytic conditions [11, 52], such as illustrated for malaria [6, 28], severe sepsis [10] or sickle cell disease [21, 29, 30]. However, the relative lack of analytical methods providing an accurate characterization of labile heme in plasma makes it difficult to prove unequivocally its direct involvement in the pathogenesis of these diseases. Here we generated and characterized a panel of heme-specific sdAbs (Fig. 1-5) providing a more accurate characterization of labile heme.

We reasoned that to detect specifically labile heme in plasma, heme-specific sdAbs should recognize heme not bound to Hb, HPX, high- or low-density lipoprotein or albumin. Therefore, the affinity of the sdAbs towards heme should be lower to the one displayed by Hb (10^{-14} M)[53], HPX (10^{-12}-10^{-13} M)[54, 55], high- or low-density lipoproteins (10^{-11}-10^{-12} M)[56] or even albumin (10^{-8} M)[5, 57]. We selected three heme-specific sdAbs, *i.e.* 1A6, 2H7 and 2H10 (Fig. 1-3), with an affinity

towards soluble heme in the rage of 10^{-7} M (Fig. 1G). Analyzes of the structural properties of the sdAb 2H10 using Spectrophotometry, Resonance Raman and FITR, suggest that this sdAb interacts with heme *via* a cysteine at the fifth ligand and possibly a lysine or a tyrosine as the sixth axial ligand (Fig. 4C-F) [36]. Heme binding promotes conformational changes in the anti-parallel β-sheets of this sdAb to presumably accommodate heme (Fig. 4D-E).

We found that heme recognition by heme-specific sdAbs is impaired as pH drops to 4-4.5 (Fig. 5A,B) being also affected by Ca^{2+} but not by the Mg^{2+} or Fe^{2+} (Fig. 3B; Fig. 5 C,D), which is consistent with similar observations for heme binding by the plasma heme scavenger hemopexin (HPX) [42][58]. Of note, while heme is bound to HPX by two histidine residues that are protonated at low pH, there are no apparent histidine residues involved in heme binding by the SdAb tested and as such the mechanism *via* which lowering pH disables heme binding to the sdAb is not clear.

We confirmed that heme accumulates in plasma during acute sterile hemolysis (Fig. 6B) and chronic hemolysis caused by *Plasmodium* infection (Fig. 7B) or by the sickle Hb (Fig. 8A). Approximately 2-8% of the heme detected in plasma (~2-5 μM) is bioavailable for internalization by bystander cells (Fig. 6D, 7E and 8C). Of note, heme is cytotoxic to parenchyma cells in this concentration range [10, 22-25, 59] arguing further for the participation of labile heme in the pathogenesis of these hemolytic conditions. Heme was not detected in plasma using the sdAb-based ELISA, suggesting that bioavailable heme is contained in a pool of labile heme bound to plasma molecules with an affinity > 10^{-7} M.

While our data is consistent with the notion that hemolytic conditions are associated with the generation of labile heme bound to plasma molecules with higher affinity than 10^{-7} M, the identity of these heme-binding molecules is not clear. Presumably, a significant proportion of the labile heme is captured by HPX (0.6–1.2 mg/mL) and by lipoproteins, which bind heme with 10^{-12} M and 10^{-10}-10^{-12} M, respectively [23] but also by albumin (43 mg/mL) that has a lower affinity (10^{-8} M) towards heme. Given their affinity towards heme (10^{-8}-10^{-12} M) these plasma proteins can capture heme from the heme-specific sdAb, as illustrated for HPX (Fig. 6G, H). This also explains why the heme-specific sdAb based ELISA does not detect labile heme in the plasma during different hemolytic conditions tested in this study.

Considering that adult mice have ~2mL of blood, ~$10x10^9$ RBC per mL and ~$3x10^8$ molecules of Hb per RBC, we estimated that 50-75% RBC lysis (Fig. 6A) should release ~10-15 mM of heme. This is consistent with the 30% decrease in $HBC_{1/2}$ following acute hemolysis (Fig. 6I), likely attributed to the saturation of plasma HPX (~10-20 µM), high (~5-11 µM) and low-density (~0,04 µM) lipoproteins and albumin (~450-600 µM) [23, 54, 59, 60] by labile heme. In contrast to acute hemolysis, chronic hemolysis associated with the development of malaria (Fig. 7) or sickle cell anemia (Fig. 8) was not associated with a reduction of plasma $HBC_{1/2}$ (Fig. 7D, 8B). Our interpretation is that a decrease in plasma $HBC_{1/2}$ is only detectable in the event of rapid release of large amounts of labile heme, overcoming the $HBC_{1/2}$ provided by high affinity plasma heme scavengers. Chronic hemolysis on the other hand is associated with a more gradual accumulation of labile heme in plasma, presumably allowing for regulatory mechanisms involving the expression of high affinity heme scavengers and the induction of heme catabolism by HO-1, as the means to prevent plasma $HBC_{1/2}$ from reaching saturation and clear excess heme. This argues for a tight regulatory mechanisms restoring systemic heme homeostasis upon hemolysis. Nevertheless, malaria (Fig. 7) and sickle cell anemia (Fig. 8) were associated with the generation of bioavailable heme that can be readily internalized by bystander cells (Fig. 7E and 8C). Our data is consistent with the notion that at the levels detected in plasma, labile heme is likely to participate in the pathogenesis of hemolytic diseases.

There are other methods that allow for the detection and characterization of labile heme in plasma, including a recently described reversed-high-performance liquid chromatography (HPLC)-based approach [61]. However, these approaches are less sensitive, as compared to the ones we describe herein, and moreover do not allow discriminating what proportion of the labile heme becomes bioavailable, which is made possible in our study based on the use of a cellular-based heme reporter assay [31, 62].

Our study shows that heme-specific sdAbs can also be used to detect intracellular heme compartmentalization (Fig. 10 and 11), showing that in human cells the majority of intracellular heme probably localizes in the mitochondria, which is consistent with the last steps of heme synthesis taking place in the mitochondria. A minor proportion of intracellular heme is also detected in the

endoplasmic reticulum of human cells (Fig. 11A) [31, 62]. This is consistent with previous studies showing that cellular labile heme concentration range at steady state from 20 to 40 nM and 2.5 nM in the cytoplasm and mitochondria of *Saccharomyces cerevisiae*, respectively [62]. The heme-specific sdAb also detected cellular heme in close vicinity of HO-1 (Fig. 11D) and bilirubin (Fig. 11E), a downstream end-product of heme catabolism. While consistent with the notion that the heme-specific sdAb recognize intracellular heme, we cannot prove that these react specifically with cellular labile heme. We are also aware that cellular fixation and permeabilization procedures do create changes in protein conformation and some level of protein unfolding, perhaps favoring the detection of loosely bound heme but also heme bound proteins with higher affinity.

Ab recognizing heme or related metalloporphyrins have long been appreciated with several of these targeting ferric mesoporphyrin [63] and increasing [64] or reducing [65] its peroxidase activity. Consistent with these findings, binding of the sdAb 2H10 to soluble heme inhibits its peroxidase activity (Fig. 9A, B), which may provide a unique opportunity to prevent the pathogenic effects of labile heme during hemolytic conditions. Given that the affinity of hemopexin for heme (10^{-12}M) is about 4-5 logs higher that that of the sdAb (10^{-7}M) or albumin (10^{-8}M), it is reasonable to assume that hemopexin should inhibit ascorbate oxidation with higher efficiency, as compared to the sdAb or to albumin. Because the sdAb 2H10 does not target related metalloporphyrins nor does it bind to heme when contained in Hb or other hemoproteins (Fig. 2 and 3) this should make its therapeutic use less toxic, as compared to approaches that target heme within hemoproteins, e.g. carbon monoxide [6, 23, 66].

EXPERIMENTAL PROCEDURES

Note: Except when indicated reagents were provide by Sigma (Sintra, Portugal).

Tetrapyrrole preparation

The concentration of different tetrapyrroles (Frontiers Scientific®, Utah, USA) was determined spectrophotometrically using appropriated solvents. Briefly, heme (*i.e.* hemin) was prepared in 0.1 M NaOH and buffered to pH 7.4 using 0.1 M HCl. Alternatively, hemin and other tetrapyrroles were

dissolved in dimethyl sulfoxide (DMSO) and concentration calculated using different wave lengths and extinction coefficients (E_{mM}), i.e. hemin (λ_{405nm}; E_{mM}= 85,82), deuteroporphyrin IX (DeutP; λ_{392nm}; E_{mM}=170), gallium protoporphyrin (GaPP; λ_{413nm}, E_{mM}=249) [67], protoporphyrin (PP; λ_{408nm}; E_{mM}=297; in 1.5 M HCl) [67], Zinc protoporphyrin (ZnPP; λ_{415nm}; E_{mM}=150, in ethanol) [67]; biliverdin (BV; λ_{377nm}; E_{mM}=51,5, in methanol) [68] and bilirubin (BR; λ_{451nm}, E_{mM}=60, in chloroform [69]. Cobalt PP (CoPP), tin PP (SnPP) and FePP IX dimethyl ester chloride (FePPCH3) concentrations in DMSO were calculated gravimetrically according to their molecular weight (MW) = 654.6, 750.26 and 679.99, respectively.

Heme biotinylation

Heme biotinylation was carried out essentially as described [70]. Briefly, hemin in dimethylformamide (DMF; 4.4 mg/mL) was incubated with 2-(1H-7-azabenzotriazol-1-yl)-1,1,3,3-tetramethyluroniumhexafluorophosphate methanaminium and N,N-diisopropylethylamine (30-60 min.; RT). N-[-5-(Hydrazinocarboxy) pentyl]-D-biotinamide (biotin) in DMSO was added (60 min.; RT) and the reaction was applied onto a C18 reverse-phase analytic HPLC column (COSMOSIL 5C18-ARII, Nacalai Tesque, Nijo Karasuma, Japan) to separate biotinylated from non-biotinylated heme and biotin. Fractions were dried (SpeedVac Plus SC110A; Vaccum System Plus UV400A) at <15ºC.

Matrix-assisted laser desorption/ionization (MALDI)-Time-of-flight mass spectrometry (TOFMS)

Hemin and biotin in 0.2 M NaOH were spotted onto the MALDI target plate and mixed 1:1 with 2,5-dihydroxybenzoic acid (DHB; 10 mg/mL) in 50% v/v acetonitrile, 5% v/v formic acid and air-dried. Heme-biotin in 50% (v/v) acetonitrile was spotted onto a MALDI plate using the Maldi matrix as described above. Data was acquired in positive reflector MS mode in a mass spectrometer (4800 plus MALDI-TOF/TOF; AB Sciex) and collected (4000 Series Explorer Software v.3.5.3; Applied Biosystems, California, USA). Mass spectrometer calibration was performed using angiotensin II (1046.542 Da), angiotensin I (1296.685 Da), Neurotensin (1672.918 Da), Adrenocorticotropic

hormone (ACTH) (1–17) (2093.087 Da) and ACTH (18–39) (2465.199 Da) (Peptide Calibration Mixture 1, LaserBio Labs, Sophia-Antipolis, France). Each reflector MS spectrum was collected using 500 laser shots per spectra and a fixed laser intensity of 3300 V.

Phage library and selection [71]

A synthetic VL sdAb phage display library previously used against several targets was used in our study [32]. The library repertoire ($8x10^9$ independent clones) was generated on a highly soluble and stable VL scaffold by randomization and accommodating a maximum of 26 aa in CDR1 and 22 aa in CDR3 [32]. The selection process was divided into four main steps: (i) incubation of phage-sdAb repertoire with heme-biotin; (ii) streptavidin capture and washing to remove non-specific phages-sdAb; (iii) heme competition for phage-sdAb elution and (iv) amplification of antigen-specific phages-sdAb. Five rounds of binding, elution and amplification were performed to select sdAbs with high binding activities and specificity. Briefly, heme-biotin (1 µg/µL) was pre-incubated (2h; RT) with the sdAb VL phage library (~10^{10}/mL). The selection procedure consisted in using streptavidin coated magnetic beads (Dynabeads; M280) to capture phages bound to heme-biotin, under a magnetic field. Unbound or low affinity bound phages were washed out (Dulbecco's Phosphate Buffered Saline (PBS) 0.5% tween 20, 5x). Bound-phages were released from the heme-biotin with a competition step by addition of excess hemin (100 µM in PBS; 1h; RT; 2x). The recovered phages were used to infect *E. coli* ER2738 (phage display optimized strain; λ_{600nm}=0.6; Biocat; 4mL; 15-30 min. 37°C). Phage-infected ER2738 bacteria were grown in Super Broth (10 µg/mL tetracycline, 100 µg/mL ampicillin) and plated in Luria Broth (LB) agar (100 µg/mL Amp) at 37ºC. Single clones were randomly selected and screened by PCR to insure the presence of VL sequences. Bacteria growing in liquid medium were then infected with VCSM13 helper phages (10^{12}-10^{13} pfu in 4 mL; 15-30 min.; 37°C), re-selected for kanamycin (100 µg/mL) resistance and left ON at 37ºC for phage production. After 16h, the selected phages were precipitated using PEG-8000 (4% w/v), NaCl (3% w/v) (1 h on ice), centrifuged (8000g; 30 min. 4°C), re-suspended (PBS, 15% Glycerol, 1 h in ice), centrifuged (16000g, 10-20 min. 4°C) and filtered (0.22µm). The resulting "purified phages" were used for one additional panning with

ten washing cycles (PBS, 0.5% Tween 20) and three more additional panning with fifteen washing cycles (PBS 0.5% Tween 20). *E. coli* (TOP10F' strain; λ_{600nm}=0.6) were infected with phages selected from the fourth panning (4mL; 15-30 min. 37°C), grown (Super Broth, 10 µg/mL tetracycline and 100 µg/mL Amp), plated (LB agar, 100 µg/mL Amp) and VL sequences confirmed by PCR. Phage-infected bacteria were grown (Super Broth, 10 µg/mL tetracycline and 100 µg/mL Amp, ON), the pComb3X phagemid DNA was extracted (Midi prep. Quiagen, Hilden, Germany), isolated and digested with SfiI (Fermentas, Portugal) for the extraction of DNA encoding sdAb fragments. These were purified from agarose gel electrophoresis, cloned into a modified pPT7-FLAG vector (Technophage SA, Lisboa, Portugal) and used to transform BL21 (DE3) *E. coli* (Promega, Wisconsin, USA). Bacterial clones were grown in auto induction medium (Novagen, Wisconsin, USA), lyzed (PBS, 20% Bugbuster, Novagen, ON, 4°C) and protein extracts were obtained (16000g, 15 min., 4°C) for selection of sdAb according to their heme binding capacity.

SdAb expression and purification

Twenty His-HA-tagged sdAbs were selected according to heme binding capacity and eleven of those were expressed and purified, essentially as described [32]. Briefly, the sdAbs cloned in a pPT7 expression vector were transformed in *E. coli* BL21 (DE3) cells and sequences were confirmed (Macrogen DNA Sequencing service, Amsterdam, the Netherlands). For protein expression, one liter of LB, (50 µg/mL Carbenicillin) was inoculated with ON culture of bacterial cells (10 mL), transformed with pPT7-VL´s plasmids and grown (37ºC) to exponential phase (λ_{600nm}=0.6-0.9). SdAb expression was induced by isopropyl β-1-thiogalactopyranoside (1mM; 6h, 37ºC). Bacteria were harvested by centrifugation (4000 g, 15 min., 4ºC) and re-suspended in equilibration buffer (50 mM HEPES, 1 M NaCl, 5 mM $CaCl_2$, 10 mM imidazole, pH 7.8; 50 mL), supplemented with protease inhibitors (Roche, Amadora, Portugal). Bacteria were lysed by sonication (20 min., ice) and inclusion bodies containing the sdAbs were recovered by centrifugation (12096*g*, 30 min., 4ºC). Pellets were washed (50mM HEPES, 1M NaCl, 10mM imidazole, 5mM $CaCl_2$, 2M urea, 1mM β-mercaptoethanol (β-ME); pH 7.8), sonicated (20 min., ice) and collected by centrifugation (12096*g*, 30 min., 4ºC).

Inclusion bodies were re-suspended in a 6 M Urea buffer (50mM HEPES, 1M NaCl, 10mM Imidazole, 5mM $CaCl_2$, 6M urea, 1mM β-ME, pH 8.0) containing benzonase (>250U, Sigma) and incubated ON (4ºC, under agitation) to allow for protein denaturation. SdAbs were purified under denaturing conditions using a His Trap Fast Flow (FF) column (GE Healthcare, Little Chalfont, United Kingdom) and washed twice (50 mM HEPES, 1M NaCl, 6M Urea, 1mM β-ME, 5mM $CaCl_2$, and 20 mM or 30 mM Imidazole; pH 7.8) to remove non specific protein contaminants. SdAb were eluted in high concentrated imidazole buffer (50 mM HEPES, 1M NaCl, 6M urea, 1mM β-ME, 5mM $CaCl_2$, 500 mM Imidazole, pH 7.8). Re-folding was achieved by step-wise dialysis, essentially as described [35]. Briefly, purified sdAb were dialyzed (24h, 4ºC) to Tris buffer (50 mM Tris-HCl, 1mM EDTA; 200 mM NaCl, 6M Urea, 10 mM β-ME) and β-ME was removed by dialysis (48h, 4ºC) to the same buffer without β-ME, allowing thiol group oxidation and consequently disulfide bond formation. SdAbs were refolded by sequential dialysis (24h, 4ºC) to Tris buffer (50 mM Tris-HCl, 1mM EDTA; 200 mM NaCl; 6M Urea), reducing Urea concentration step wise from 3, 2, 1, 0.5 and 0 M. Dialyses to buffers containing 1M and 0.5M Urea were supplemented with 0.4 mM oxidized glutathione (GSSG) and 4 mM reduced glutathione (GSH) plus 400 mM L-arginine to promote protein refolding (30). SdAbs were centrifuged (4000*g*, 4ºC, 10 min.), to remove protein precipitates, aliquoted and stored (-80ºC) until used. SdAbs purity was assessed by Sodium dodecyl sulfate-polyacrylamide gel electrophoresis (SDS-PAGE) gel with 15% acrylamide under denaturing conditions followed by based Coomassie-based stain (Instant Blue, 30 min., RT, Gentaur, Kampenhout, Belgium.) and by Western blotting.

SdAb biotinylation

Briefly, sdAb where incubated with 20-fold molar excess of biotin (2h, ice) in PBS using EZ-Link NHS-PEG4-Biotinylation kit (Pierce by Thermofisher, Massachusetts, United States). Free biotin and free sdAb were removed using a desalting column (Thermo Zeba Spin Desalting column, Pierce) (1000*g*, 2 min.), pre-equilibrated in PBS. SdAb biotinylation was confirmed using 4'-hydroxyazobenzene-2-carboxylic acid (HABA) assay. Briefly, biotinylated-sdAb was mixed (1/10)

with a HABA/Avidin (0.5 mg/mL avidin, 0.3 mM HABA, PBS) in a 96 well plate and λ_{500nm} measured in a microplate reader (Victor^3 Multilabel Readers, Perkin Elmer). Biotinylated-sdAbs were stored at -80ºC until used.

Western Blotting

Proteins were subjected to 15% SDS-PAGE gel electrophoresis (15 V, 60 min.), transferred into methanol activated polyvinyldifluoridine membrane (2 min.), washed (3x in H_2O, 3x T-TBS; 20 mM Tris pH 7.5, 150 mM, 0.05% Tween-20) and blocked (5%-skim milk in T-TBS; 1h, ON; RT). SdAbs were detected using a horseradish peroxidase (HRP)-conjugated rat anti-HA monoclonal Ab (mAb) (1/2000, Roche ®). Peroxidase activity was revealed using SuperSignal West Pico Chemiluminescent substrate (Pierce) in a photoradiograph (Kodak Biomax Light Film; Eastman Kodak, New York, USA). ExPASy - ProtParam tool was used to estimate the MW and isoelectronic point of sdAbs.

ELISA

Hemin (100 µM) in carbonate buffer (0.1M $NaHCO_3$, pH 8.6) was used bound to 96 well plates (Costar 3690) (1h, RT or ON at 4ºC), washed (3x, PBS, 0.1% Tween 20), blocked in protein free blocking buffer (Pierce; 1h, RT) and washed (4x, PBS, 0.1% Tween 20). Bacterial supernatants or purified sdAbs were added (1h 30 min., RT, diluted in PBS), plates were washed (5x PBS, 0.1% Tween 20) and heme-bound sdAbs were detected using a rat anti-HA mAb (3F10; Roche; 0.1µg/mL) in protein-free blocking buffer. Plates were washed (5x PBS, 0.1% Tween 20) and the rat anti-HA mAb was detected using an alkaline phosphatase labeled rabbit anti-whole rat IgG (Sigma) polyclonal Ab (1 h, RT, 1/2000) in protein free blocking buffer. Alkaline phosphatase was revealed with para-Nitrophenylphosphate (pNPP, 1mg/mL; Sigma). Absorbance was measured in a microplate reader at λ_{450nm} (Victor^3 Multilabel Readers, Perkin Elmer).

To measure the total amount of protein in sdAb supernatants, 96 well plates (Costar 3690, Sigma) were coated with the sdAb supernatant in 50 mM carbonate/bicarbonate buffer, pH 9.6 (1h, RT or 16h, 4ºC). The rest of the procedure was performed as described above. Absorbance was measured in a microplate reader at λ_{450nm}.

To measure labile heme, 96 well plates were coated with SdAb 1A6 (0.3-5 µg/mL) in 50 mM carbonate/bicarbonate buffer, pH 9.6 (16h, 4ºC), washed (5x, PBS 0.1% Tween 20) and blocked (2h, RT) with protein free blocking buffer. Plates were incubated with hemin (0.15-5 µM in PBS), used as standard or with plasma (1h 30 min., RT). Plates were washed (5x, PBS, 0.1% Tween 20) and heme was detected using biotinylated 2H7 sdAb (2.5-5 ng/µL) in PBS. Plates were washed (5x, PBS, 0.1% Tween 20) and biotinylated sdAb was detected using Alkaline phosphatase conjugated with ExtrAvidin (1/2500, Sigma) in protein blocking buffer. Plates were washed (5x, PBS 0.1% Tween 20) and Alkaline phosphatase was revealed using pNPP (1mg/mL; Sigma). Absorbance was measured in a microplate reader at λ_{450nm}.

Biacore

SdAbs affinity towards heme was determined using surface plasmon resonance (SPR) (BIAcore 2000, BIAcore Inc. by Ge Healthcare). Briefly, sdAbs were captured on a CM5 chip using amine coupling at ~800 resonance units (RU). Heme (0-3000 nM) was injected for 4 min and sdAb-bound heme was allowed to dissociate (10 min.) before matrix regeneration (10 mM Glycine, pH 2.5). The signal was subtracted from that of an immobilized cell to generate sensorgrams of the amount of bound heme as a function of time. The running buffer, HBS-P (0.01 M HEPES pH 7.4, 0.15 M NaCl, 0.005% v/v Surfactant P20; BIAcore) was used for all sample dilutions. BIAcore kinetic evaluation software (version 3.1) was used to determine dissociation constant (KD) from the association and dissociation rates using a one-to-one binding model. An irrelevant sdAb was used as negative control.

SdAb pull-down assay

SdAb binding to soluble hemin was assessed by a pull-down assay. Briefly, sdAbs were incubated (5h, 4ºC, agitation) with heme-biotin and half of the reaction mixture was incubated (2h, RT, agitation) with of Streptavidin-Dynabeads (M-280 Streptavidin, Invitrogen by Thermofisher), previously blocked (5h, RT) with protein free blocking buffer (Pierce). Mixture was washed (3x; 5 min.; PBS, 0.05% Tween 20) and magnetic beads were captured (5 min. magnetic field) according to the manufacture's instructions. SdAbs-heme-biotin complexes were collected (1 min., magnetic field)

and incubated (20 min., 100ºC, agitation) in loading buffer (50mM Tris-HCl pH 6.8, 2%SDS, 10% Glycerol, 1% β-ME, 12,5 mM EDTA, 0.02% Bromophenol blue) (pull-down). The other half of the reaction mixture was denatured (100ºC, 10 min.) in loading buffer. Proteins were applied into a 15% SDS-PAGE gel under denaturing conditions and stained with a Coomassie-based stain (Instant Blue, Gentaur, 30 min., RT). Alternatively, sdAb were detected by Western blotting using a rat anti-HA horseradish peroxidase (HRP) conjugated mAb (1/5000, Roche ®) (1h, RT).

Hemopexin (HPX)

Apo-HPX was isolated from rabbit serum, as described [10, 72](kind gift from Dr. Ann Smith, University of Missouri-K.C., Kansas City, MO). Binding of HPX to heme was confirmed by UV-Vis spectrophotometry of the apo-protein or heme-HPX complexes; the concentration of the protein and equimolar heme binding were quantified, as described [73].

Heme/sdAb complexes

SdAbs in PBS were incubated with 2x molar excess hemin in NaOH/HCl pH 7.4 (ON, 4ºC). Free heme and free sdAb were separated using a PD10 column (GEHealthcare) pre-equilibrated in PBS. Heme binding to the sdAb was confirmed spectrophotometrically. Concentration of sdAb-heme complex was determined using formic acid assay, as described bellow (total heme). Total amount of protein was determined using Quick Start Bradford Protein Assay (Biorad, California, USA), according to the manufacture's instructions.

Spectroscopy assays

UV-Visible spectra were recorded (PerkinElmer Lambda 25, UV/Vis spectrometer) using a concentration of 10 µM of sdAb in PBS. Increasing amount of hemin in 0.1M NaOH (pH 7.4) were added and incubated (5 min.) before recording the next spectra. Resonance Raman (RR) spectra were obtained using Raman spectrometer (Join Yvon U1000) coupled to a confocal microscope equipped with 1,200 lines/mm grating and a liquid nitrogen-cooled back-illuminated charge coupled device (CCD) detector. The spectra of 40 µM protein bound to heme and 50 µM heme in PBS buffer were

obtained using a rotating cell (Hellma, Müllheim, Germany) to avoid photoreduction and measured with λ_{413nm} excitation line from a Krypton ion laser (Coherent Innova 302) with 4.5 mW laser power and 60 s accumulation time, at RT; typically 10 spectra were co-added to improve signal to noise ratio. After polynomial background subtraction, spectra were subjected to component analysis to determine the bandwidths and positions, using in-house created software. Circular Dichroism (CD) Spectroscopy measurements were performed using a Jasco J-815 spectropolarimeter equipped with a Peltier-controlled thermostated cell support. CD spectra were recorded with sdAb 2H10 (240 µg/mL in 35% 50mM TRIS, 200 mM NaCl, 0.1 mM EDTA, 10% glycerol; pH 7.4 in PBS). Spectra were collected (50nm/min.) and acquired (10x) to improve the signal to noise ratio. Attenuated total reflectance (ATR) Fourier transform infrared (FTIR) spectra were measured on a Bruker IFS 66/S spectrometer equipped with a MCT detector and a thermostatized Harrick BioATR II cell. All measurements were obtained using an ATR cell with sdAb 2H10 (700 µg/mL in 50mM TRIS, 200 mM NaCl, 0.1 mM EDTA, 10% glycerol at pH 7.4) dissolved in PBS (1x), with or without heme. Each spectrum comprises the mean of 150 scans taken at a resolution of 4 cm^{-1}. Spectral assignments for specific secondary structure elements were made as in [41].

Mice

Mice were maintained under SPF conditions and experiments approved by the Ethics Committee of the Instituto Gulbenkian de Ciência, Direção Geral de Alimentação e Veterinária (Decreto-Lei nº 113/2013) and European legislation (Directive 2010/63/EU). C57BL/6J mice were obtained from the Instituto Gulbenkian de Ciência's Animal Facility. C57BL/6xSv129 hα/hα::β^A/β^A, hα/hα::β^A/β^S and hα/hα::β^S/β^S mice [43] were obtained from Jackson laboratories (Reference 013071).

pH titration

To address the effect of pH on heme binding by sdAb, assays were performed, essentially as described [74]. Briefly, sdAb (10 µM in PBS) were allowed to bind hemin (10 µM; pH 7, 15-20 min, RT) and pH was titrated down to 4.0-4.5 using 0.5 M HCl and restored thereafter using 0.5M KOH (RT). To evaluate the effect of divalent cations, sdAbs bound to heme were first titrated down using

0.5 M HCl, followed by the addition of $CaCl_2$ or $MgCl_2$ (3 mM) at pH 4.0-4.5 and then the pH was titrated up to neutral using 0.5M KOH (RT). UV-visible spectra were recorded (PerkinElmer Lambda 25, UV/Vis spectrometer). Background of the spectra was corrected using the software OriginPro 8®.

Phenylhydrazine

Adult C57BL/6 mice were injected (s.c.) with freshly prepared phenylhydrazine (Sigma) (1xPBS, pH7.4; 90 mg/Kg; body weight).

***Plasmodium* infection**

Adult C57BL/6 mice were infected intraperitoneally (i.p.) with $2x10^6$ *Pcc* AS strain per mouse and parasitemias were determined by Giemsa-stained blood smears and monitored daily, as described [22, 24].

Mouse plasma

Obtained by cardiac puncture (heparin or EDTA), centrifuged (2x; 1600g, 5min., 4ºC) and stored (-80ºC).

Total heme

Heme concentration was measured essentially as described [75]. Briefly, samples were diluted in H_2O in 96 well plates, formic acid (150 µL/well; 98-100%, Merck) was added and absorbance was measured at λ_{405nm} using a microplate reader (Victor^3 Multilabel Readers, Perkin Elmer). Heme concentration was determined by comparison to a hemin standard curve (0.5-16 µM in H_2O).

Bioavailable heme

Bioavailable heme was measured using a previously described cellular heme reporter assay based on heme dependent HRP activity [12, 31]. Briefly, HEK293 cells (ATCC; $5x10^4$ cells/well in a 24 well plate) were grown (ON; DMEM, 10% FBS, 1% penicillin 10000 U/mL, streptomycin 10000 µg/mL) and transiently transfected (4-6h, Lipofectamin 2000; Invitrogen) with an expression vector encoding

the HRP gene under the control of the EF-1α promoter (pEF5/FRT/V5-DEST-Golgi-HRP) in opti-MEM reduced serum (Gibco by thermofisher) [12]. Expression of HRP was confined to the Golgi with a targeting sequence from galactosyltransferase [12, 31]. Control HEK293 cells were transiently transfected with the pEF5/FRT/V5-DEST vector [12, 31]. Transfected cells were cultured (24h) in DMEM (10% heme-depleted FBS) with or without succinylacetone (SA; 0.5 mM) to block endogenous heme synthesis. Cells were washed and treated with hemin (ON) in opti-MEM containing 0.5 mM SA and peroxidase activity was assessed as a red-out of cellular heme content. Briefly, cells were lysed (20 mM HEPES pH 7.4, 150 mM NaCl, 0.5% Triton X-100, 2,5X protease inhibitor cocktail set; Calbiochem®) (ice, 20 min.), centrifuged (13.500 rpm, 4ºC, 5min.) and peroxidase activity was quantified in a 96 well plate using 3,3',5,'-Tetramethylbenzidine (TMB) substrate reagent set (BD OptEIA by thermofisher). Reaction was stopped (2N H_2SO_4) and absorbance was measured in a microplate reader at λ_{450nm} (Victor^3 Multilabel Readers, Perkin Elmer). Peroxidase activity was determined based on the calibration curve generated with the serial dilution of HRP (type IV, Sigma) and normalized to protein expression (Quick Start Bradford Protein Assay; Biorad). HRP concentration was determined based on Beer-Lambert law using the extinction coefficient (λ_{403nm}; E_{mM}=100).

Heme depleted medium

Depletion of heme from culture medium was performed as described [76]. Briefly, DMEM (Life Technologies) was supplemented with 10% heat inactivated fetal bovine serum (FBS; Life Technologies by Thermofisher) pre-depleted from heme using ascorbic acid (10 mM; 37ºC, 50 rpm) until λ_{405nm}=0.6-0.8 (~7 h), dialyzed (3x) in sterile PBS and filtered (0.2µm). Final culture medium was supplemented with 1% penicillin (10000 U/mL) and streptomycin (10000 µg/mL).

Heme binding capacity ($HBC_{1/2}$)

The assay is based on the following principle: Plasma is incubated *in vitro* with increasing concentrations of heme (1h30, RT, agitation), until saturation of heme-binding molecules (with an affinity towards heme higher than 10^{-7} M). The heme-specific sdAb-based ELISA is used, as described above, to detect excess heme. The concentration of heme required to reduce by 50% the plasma heme-binding capacity is defined as $HBC_{1/2}$.

Heme competition assays

SdAbs (2.5 µg/mL) were pre-incubated (90 min., RT, mild agitation) with tetrapyrroles or hemoproteins and used to detect solid-phase bound heme by ELISA, as described above.

Ascorbate oxidation assay

We adapted a previously described assay [77] as a readout for the oxidation activity of heme in the absence or presence of albumin or heme-specific sdAb. Briefly, the reaction was initiated by the addition of heme (0-5 µM), without or with protein/sdAb (0-5µM) and hydrogen peroxide (800µM), to ascorbate (10 µM) in PBS pH 7.4 containing a metal chelator DETAPAC (50 µM) that does not inhibit heme mediated oxidation. The reaction was carried out under air at 37ºC and after a certain time, stopped by the addition of one volume of 0.5% metaphosphoric acid to one volume of reaction mix. The final solution was centrifuged and the supernatant collected and analyzed using HPLC with electrochemical detection [78].

Heme-biotin pull-down assay

SdAb 2H10 was incubated (30-60 min, 4ºC, agitation) with heme-biotin and HPX was added to the mixture at 1/6 SdAb/HPX molar ratio (30-60 min, 4ºC, agitation). To evaluate the ability of HPX to bind heme-biotin, HPX was incubated (30-60 min, 4ºC, agitation) with heme-biotin. Half of the reaction mixture was incubated (2h, RT, agitation) with Streptavidin-Dynabeads (M-280 Streptavidin, Invitrogen), previously blocked (5h, RT) with protein free blocking buffer (Pierce). The reaction mixture was washed (3x; 5 min.; PBS, 0.05% Tween 20), magnetic beads were captured (5 min.

magnetic field) according to the manufacture's instructions and incubated (20 min., 100ºC, agitation) in loading buffer (50mM Tris-HCl pH 6.8, 2%SDS, 10% Glycerol, 1% β-ME, 12,5 mM EDTA, 0.02% Bromophenol blue). The other half of the reaction mixture was denatured (100ºC, 10 min.) in loading buffer. Reaction mixtures in loading buffer were applied into a 15% SDS-PAGE gel under denaturing conditions and stained with a coomassie-based stain (Instant Blue, Gentaur, 30 min., RT).

Intracellular heme detection by immunofluorescence

HeLa (ATCC) cells were grown (24h) in DMEM (10% FBS, 1% penicillin 10000 U/mL, streptomycin 10000 µg/mL; Life Technologies), seeded onto coverslips in a 24 well plate until 80% confluence. Cells were washed (1x, PBS), incubated (5min., RT) in a hypotonic solution (85.5 mM NaCl, 5 mM $MgCl_2$, pH 7.0), fixed (ice cold methanol, 10 min., -20ºC or 4% paraformaldehyde, 10 min at RT), washed (1x, PBS), permeabilized (PBS, 0.1% triton X-100, 5 min.), washed (3x, PBS) and blocked (Protein-Free Blocking Buffer, Pierce, 1h, RT). For intracellular heme detection cells were incubated with heme-specific sdAbs (2,5 ng/µL; 3h, RT), washed (3x, blocking buffer) and incubated (1h, RT) with Alexa Fluor ®647 conjugated anti-HA Ab (clone 6E3; Cell Signaling Technology). Cells were washed (3x, PBS, 1x milli-Q Water), DNA was stained with DAPI (Sigma), dried and mounted with coversplips in Mowiol-Dabco media with DAPI. Images were acquired on a Leica DMRA2 upright microscope, equipped with a CoolSNAP HQ CCD camera, using a 100x 1.4NA Oil immersion objective, DAPI + CY5 fluorescence filtersets, controlled with the MetaMorph V7.5.1/ software. The analysis was done with ImageJ (Rasband, W.S., ImageJ, U. S. National Institutes of Health, Bethesda, Maryland, USA, http://imagej.nih.gov/ij/, 1997-2014). When indicated cells were co-immunostained with an anti-Calnexin rabbit Ab, an integral endoplasmic reticulum protein (clone C4731, Sigma), anti-early endosome antigen 1 (EEA-1) rabbit Ab, to localize early endosomes, phalloidin–tetramethylrhodamine B isothiocyanate phalloidin, a toxin that binds F-actin (P1951, Sigma), anti-bilirubin mAb (A420, Dojindo) or anti-HO-1 polyclonal Ab (SPA-896, Stressgen). Mitochondria were stained with MitoTracker® Red (Life Technologies). Confocal Z-series stacks were acquired on a Leica SP5 Live upright microscope, using a 63x 1.3NA Oil immersion objective, with DAPI + Fluorescein isothiocyanate (FITC) + CY5 or DAPI +

Tetramethylrhodamine (TRITC) + CY5 laser lines, and spectral detection adjusted for the emission of the respective fluorochromes, controlled with the Leica software. The analysis was done with ImageJ (Rasband, W.S., ImageJ, U. S. National Institutes of Health, Bethesda, Maryland, USA, http://imagej.nih.gov/ij/, 1997-2014).

Intracellular heme detection by flow cytometry

HeLa cells were tripsinized (0.05% Trypsin-EDTA, Life Technologies), washed (1x, PBS), fixed (ice cold methanol, 10 min., -20ºC), re-suspended, washed (1x, PBS), permeabilized (PBS, 0.1% triton X-100,5 min.), washed (1x, PBS) and blocked (Protein-Free Blocking Buffer; Pierce) (1h, RT). Intracellular heme was detected using anti-heme sdAb (2.5 µg/mL in blocking buffer, 2h30min., RT, shaking) followed by Alexa Fluor® 647 conjugated HA-Tag (6E3) mouse mAb (1/200, Cell Signaling Technology). Cells were washed (1x, PBS), re-suspended (PBS) and acquired in a FACScan (Becton Dickinson) with CellQuest software (BD Biosciences). The analysis was done with FlowJo (Tree Star, Inc.).

Statistical Analysis

When comparing the means of more than two experimental groups, we used analysis of variance (ANOVA) and significance between groups was estimated using Bonferroni post-test, when Gaussian distribution was confirmed. For samples with non-Gaussian distribution, comparison between experimental groups was performed using a Kruskal-Wallis test, followed by post-test Dunns to compare all paired groups. Statistical analyses were performed using the GraphPad v.5.0a software (Prism), and p values were represented as *$p < 0.05$, ** $p < 0.01$, ***$p<0.001$.

ACKNOWLEDGEMENTS: Dr. Ana Maria Varela Coelho and Renata Soares at Mass spectrometry and analytic services units of the Instituto de Tecnologia Química e Biológica (ITQB). Pierre Crozet and Jorge Carneiro for help in analysis of $HBC_{1/2}$. Dr. C Suarna for help with the ascorbate oxidation studies. The inflammation group at Instituto Gulbenkian de Ciência for critical discussion and comments. This work was supported by Fundação para a Ciência e Tecnologia (FCT), Portugal,

(RECI-IMI-IMU-0038-2012; PTDC/SAU-TOX/116627/2010; HMSP-ICT/0018/2011 to MPS, SFRH/BD/44828/2008 to ZG, SFRH/BPD/47477/2008 to SSL, PTDC/SAU-FAR/119173/2010 to JG, IF/01010/2013/CP1183/CT0001 to F.A.S), from ERC-2011-AdG 294709-DAMAGECONTROL to MPS, and NHMRC Senior Principal Research Fellowship 1003484 to RS.

AUTHORSHIP CONTRIBUTIONS: ZG co-designed, performed or co-performed all the experimental work and analyzed the data with the exception of ascorbate oxidation designed and performed by RS and immunofluorescence and Flow cytometry assays designed and performed by ARC. SR contributed in the malaria experiments. JG and FAS conceived and designed the synthetic phage display library and contributed critically to screening of sdAbs by Phage display technology. CMG and SSL contributed with the analysis by Circular Dichroism and Attenuated total reflectance Fourier transform infrared spectroscopy. ST and ZG performed Resonance Raman analysis. OI and ZG performed heme biotinylation. IH and XY developed the Golgi-HRP assay and assisted ZG; MPS conceived, designed, supervised the study and wrote the manuscript with ZG. All the authors read, corrected, comment and approved the manuscript.

REFERENCES

1. Fischer, H. & Zeile, K. (1929) Synthese des haematoporphyrins, protoporphyrins und haemins, *Justus Liebigs Annalen der Chemie* **468**, 98-116.

2. Tsiftsoglou, A. S., Tsamadou, A. I. & Papadopoulou, L. C. (2006) Heme as key regulator of major mammalian cellular functions: molecular, cellular, and pharmacological aspects, *Pharmacol Ther.* **111**, 327-45.

3. Moncada, S. & Erusalimsky, J. D. (2002) Does nitric oxide modulate mitochondrial energy generation and apoptosis?, *Nat Rev Mol Cell Biol.* **3**, 214-20.

4. Dioum, E. M., Rutter, J., Tuckerman, J. R., Gonzalez, G., Gilles-Gonzalez, M. A. & McKnight, S. L. (2002) NPAS2: a gas-responsive transcription factor, *Science.* **298**, 2385-7.

5. Severance, S. & Hamza, I. (2009) Trafficking of heme and porphyrins in metazoa, *Chem Rev.* **109**, 4596-616.

6. Pamplona, A., Ferreira, A., Balla, J., Jeney, V., Balla, G., Epiphanio, S., Chora, A., Rodrigues, C. D., Gregoire, I. P., Cunha-Rodrigues, M., Portugal, S., Soares, M. P. & Mota,

M. M. (2007) Heme oxygenase-1 and carbon monoxide suppress the pathogenesis of experimental cerebral malaria, *Nat Med.* **13**, 703-10.

7. Hebbel, R. P., Morgan, W. T., Eaton, J. W. & Hedlund, B. E. (1988) Accelerated autoxidation and heme loss due to instability of sickle hemoglobin, *Proc Natl Acad Sci U S A.* **85**, 237-41.

8. Balla, J., Jacob, H. S., Balla, G., Nath, K., Eaton, J. W. & Vercellotti, G. M. (1993) Endothelial-cell heme uptake from heme proteins: induction of sensitization and desensitization to oxidant damage, *Proceedings of the National Academy of Sciences of the United States of America.* **90**, 9285-9.

9. Bunn, H. F. & Jandl, J. H. (1968) Exchange of heme among hemoglobins and between hemoglobin and albumin, *J Biol Chem.* **243**, 465-75.

10. Larsen, R., Gozzelino, R., Jeney, V., Tokaji, L., Bozza, F. A., Japiassu, A. M., Bonaparte, D., Cavalcante, M. M., Chora, A., Ferreira, A., Marguti, I., Cardoso, S., Sepulveda, N., Smith, A. & Soares, M. P. (2010) A central role for free heme in the pathogenesis of severe sepsis, *Sci Transl Med.* **2**, 51ra71.

11. Ferreira, A., Balla, J., Jeney, V., Balla, G. & Soares, M. P. (2008) A central role for free heme in the pathogenesis of severe malaria: the missing link?, *J Mol Med.* **86**, 1097-111.

12. White, C., Yuan, X., Schmidt, P. J., Bresciani, E., Samuel, T. K., Campagna, D., Hall, C., Bishop, K., Calicchio, M. L., Lapierre, A., Ward, D. M., Liu, P., Fleming, M. D. & Hamza, I. (2013) HRG1 is essential for heme transport from the phagolysosome of macrophages during erythrophagocytosis, *Cell Metab.* **17**, 261-70.

13. Smith, D. W. (1980) The molecular biology of mammalian hemoglobin synthesis, *Ann Clin Lab Sci.* **10**, 116-22.

14. Balla, G., Vercellotti, G., Eaton, J. W. & Jacob, H. S. (1990) Heme uptake by endothelium synergizes polymorphonuclear granulocyte-mediated damage, *Trans Assoc Am Physicians.* **103**, 174-9.

15. Balla, G., Jacob, H. S., Balla, J., Rosenberg, M., Nath, K., Apple, F., Eaton, J. W. & Vercellotti, G. M. (1992) Ferritin: a cytoprotective antioxidant strategem of endothelium, *Journal of Biological Chemistry.* **267**, 18148-53.

16. Soares, M. P. & Bozza, M. T. (2016) Red alert: labile heme is an alarmin, *Curr Opin Immunol.* **38**, 94-100.

17. Figueiredo, R. T., Fernandez, P. L., Mourao-Sa, D. S., Porto, B. N., Dutra, F. F., Alves, L. S., Oliveira, M. F., Oliveira, P. L., Graca-Souza, A. V. & Bozza, M. T. (2007) Characterization of heme as activator of Toll-like receptor 4, *J Biol Chem.* **282**, 20221-9.

18. Dutra, F. F., Alves, L. S., Rodrigues, D., Fernandez, P. L., de Oliveira, R. B., Golenbock, D. T., Zamboni, D. S. & Bozza, M. T. (2014) Hemolysis-induced lethality involves inflammasome activation by heme, *Proc Natl Acad Sci U S A*.

19. Porto, B. N., Alves, L. S., Fernandez, P. L., Dutra, T. P., Figueiredo, R. T., Graca-Souza, A. V. & Bozza, M. T. (2007) Heme induces neutrophil migration and reactive oxygen species generation through signaling pathways characteristic of chemotactic receptors, *J Biol Chem.* **282**, 24430-6.

20. Fernandez, P. L., Dutra, F. F., Alves, L., Figueiredo, R. T., Mourao-Sa, D., Fortes, G. B., Bergstrand, S., Lonn, D., Cevallos, R. R., Pereira, R. M., Lopes, U. G., Travassos, L. H., Paiva, C. N. & Bozza, M. T. (2010) Heme amplifies the innate immune response to microbial molecules through spleen tyrosine kinase (Syk)-dependent reactive oxygen species generation, *J Biol Chem.* **285**, 32844-51.

21. Belcher, J. D., Chen, C., Nguyen, J., Milbauer, L., Abdulla, F., Alayash, A. I., Smith, A., Nath, K. A., Hebbel, R. P. & Vercellotti, G. M. (2014) Heme triggers TLR4 signaling leading to endothelial cell activation and vaso-occlusion in murine sickle cell disease, *Blood.* **123**, 377-90.

22. Seixas, E., Gozzelino, R., Chora, A., Ferreira, A., Silva, G., Larsen, R., Rebelo, S., Penido, C., Smith, N. R., Coutinho, A. & Soares, M. P. (2009) Heme oxygenase-1 affords protection against noncerebral forms of severe malaria, *Proc Natl Acad Sci U S A.* **106**, 15837-42.

23. Gozzelino, R., Jeney, V. & Soares, M. P. (2010) Mechanisms of cell protection by heme oxygenase-1, *Annu Rev Pharmacol Toxicol.* **50**, 323-54.

24. Gozzelino, R., Andrade, B. B., Larsen, R., Luz, N. F., Vanoaica, L., Seixas, E., Coutinho, A., Cardoso, S., Rebelo, S., Poli, M., Barral-Netto, M., Darshan, D., Kuhn, L. C. & Soares, M. P. (2012) Metabolic adaptation to tissue iron overload confers tolerance to malaria, *Cell Host Microbe.* **12**, 693-704.

25. Gozzelino, R. & Soares, M. P. (2014) Coupling heme and iron metabolism via ferritin H chain, *Antioxid Redox Signal.* **20**, 1754-69.

26. Weis, S., Carlos, A. R., Moita, M. R., Singh, S., Blankenhaus, B., Cardoso, S., Larsen, R., Rebelo, S., Schäuble, S., Del Barrio, L., Mithieux, G., Rajas, F., Lindig, S., M., B. & M.P., S. (2017) Metabolic adaptation establishes disease tolerance to sepsis, *Cell.* **169**, 1263–1275.

27. Roumenina, L. T., Rayes, J., Lacroix-Desmazes, S. & Dimitrov, J. D. (2016) Heme: Modulator of Plasma Systems in Hemolytic Diseases, *Trends Mol Med.* **22**, 200-13.

28. Ferreira, A., Marguti, I., Bechmann, I., Jeney, V., Chora, A., Palha, N. R., Rebelo, S., Henri, A., Beuzard, Y. & Soares, M. P. (2011) Sickle Hemoglobin Confers Tolerance to Plasmodium Infection, *Cell.* **145**, 398–409.

29. Vinchi, F., De Franceschi, L., Ghigo, A., Townes, T., Cimino, J., Silengo, L., Hirsch, E., Altruda, F. & Tolosano, E. (2013) Hemopexin therapy improves cardiovascular function by preventing heme-induced endothelial toxicity in mouse models of hemolytic diseases, *Circulation.* **127**, 1317-29.

30. Ghosh, S., Adisa, O. A., Chappa, P., Tan, F., Jackson, K. A., Archer, D. R. & Ofori-Acquah, S. F. (2013) Extracellular hemin crisis triggers acute chest syndrome in sickle mice, *J Clin Invest.* **123**, 4809-20.

31. Yuan, X., Rietzschel, N., Kwon, H., Walter Nuno, A. B., Hanna, D. A., Phillips, J. D., Raven, E. L., Reddi, A. R. & Hamza, I. (2016) Regulation of intracellular heme trafficking revealed by subcellular reporters, *Proc Natl Acad Sci U S A.* **113**, E5144-52.

32. Cunha-Santos, C., Figueira, T. N., Borrego, P., Oliveira, S. S., Rocha, C., Couto, A., Cantante, C., Santos-Costa, Q., Azevedo-Pereira, J. M., Fontes, C. M., Taveira, N., Aires-Da-Silva, F., Castanho, M. A., Veiga, A. S. & Goncalves, J. (2016) Development of synthetic light-chain antibodies as novel and potent HIV fusion inhibitors, *AIDS.* **30**, 1691-701.

33. Goncalves, J., Silva, F., Freitas-Vieira, A., Santa-Marta, M., Malho, R., Yang, X., Gabuzda, D. & Barbas, C., 3rd (2002) Functional neutralization of HIV-1 Vif protein by intracellular immunization inhibits reverse transcription and viral replication, *J Biol Chem.* **277**, 32036-45.

34. Barbas, C. F., Burton, D. R., Scott, J. K. & Silverman, G. J. (2001) *Phage Display A Laboratory Manual*, Cold Spring Harbor Laboratory, New York.

35. Umetsu, M., Tsumoto, K., Hara, M., Ashish, K., Goda, S., Adschiri, T. & Kumagai, I. (2003) How additives influence the refolding of immunoglobulin-folded proteins in a stepwise dialysis system. Spectroscopic evidence for highly efficient refolding of a single-chain Fv fragment, *J Biol Chem.* **278**, 8979-87.

36. Li, T., Bonkovsky, H. L. & Guo, J. T. (2011) Structural analysis of heme proteins: implications for design and prediction, *BMC Struct Biol.* **11**, 13.

37. Pearson, A. R., Elmore, B. O., Yang, C., Ferrara, J. D., Hooper, A. B. & Wilmot, C. M. (2007) The crystal structure of cytochrome P460 of Nitrosomonas europaea reveals a novel cytochrome fold and heme-protein cross-link, *Biochemistry.* **46**, 8340-9.

38. McDonagh, A. F. (2001) Turning green to gold, *Nature Structural Biology.* **8**, 198-200.

39. Marvin, K. A., Kerby, R. L., Youn, H., Roberts, G. P. & Burstyn, J. N. (2008) The transcription regulator RcoM-2 from Burkholderia xenovorans is a cysteine-ligated hemoprotein that undergoes a redox-mediated ligand switch, *Biochemistry.* **47**, 9016-28.

40. Mouro, C., Jung, C., Bondon, A. & Simonneaux, G. (1997) Comparative Fourier transform infrared studies of the secondary structure and the CO heme ligand environment in cytochrome P-450cam and cytochrome P-420cam, *Biochemistry.* **36**, 8125-34.

41. Barth, A. & Zscherp, C. (2002) What vibrations tell us about proteins, *Q Rev Biophys.* **35**, 369-430.

42. Jeney, V., Ramos, S., Bergman, M. L., Bechmann, I., Tischer, J., Ferreira, A., Oliveira-Marques, V., Janse, C. J., Rebelo, S., Cardoso, S. & Soares, M. P. (2014) Control of disease tolerance to malaria by nitric oxide and carbon monoxide, *Cell Rep.* **8**, 126-36.

43. Wu, L. C., Sun, C. W., Ryan, T. M., Pawlik, K. M., Ren, J. & Townes, T. M. (2006) Correction of sickle cell disease by homologous recombination in embryonic stem cells, *Blood.* **108**, 1183-8.

44. Muller-Eberhard, U., Javid, J., Liem, H. H., Hanstein, A. & Hanna, M. (1968) Plasma concentrations of hemopexin, haptoglobin and heme in patients with various hemolytic diseases, *Blood.* **32**, 811-5.

45. Vinchi, F., Costa da Silva, M., Ingoglia, G., Petrillo, S., Brinkman, N., Zuercher, A., Cerwenka, A., Tolosano, E. & Muckenthaler, M. U. (2015) Hemopexin therapy reverts heme-induced pro-inflammatory phenotypic switching of macrophages in a mouse model of sickle cell disease, *Blood*.

46. Ascenzi, P., Bocedi, A., Visca, P., Altruda, F., Tolosano, E., Beringhelli, T. & Fasano, M. (2005) Hemoglobin and heme scavenging, *IUBMB Life.* **57**, 749-59.

47. Soares, M. P. & Weiss, G. (2015) The Iron age of host-microbe interactions, *EMBO Rep.* **16**, 1482-500.

48. Soares, M. P. & Hamza, I. (2016) Macrophages and Iron Metabolism, *Immunity.* **44**, 492-504.

49. Balla, J., Balla, G., Jeney, V., Kakuk, G., Jacob, H. S. & Vercellotti, G. M. (2000) Ferriporphyrins and endothelium: a 2-edged sword-promotion of oxidation and induction of cytoprotectants, *Blood.* **95**, 3442-50.

50. Balla, G., Vercellotti, G. M., Muller-Eberhard, U., Eaton, J. & Jacob, H. S. (1991) Exposure of endothelial cells to free heme potentiates damage mediated by granulocytes and toxic oxygen species, *Lab Invest.* **64**, 648-55.

51. Graca-Souza, A. V., Arruda, M. A., de Freitas, M. S., Barja-Fidalgo, C. & Oliveira, P. L. (2002) Neutrophil activation by heme: implications for inflammatory processes, *Blood.* **99**, 4160-5.

52. Schaer, D. J., Buehler, P. W., Alayash, A. I., Belcher, J. D. & Vercellotti, G. M. (2013) Hemolysis and free hemoglobin revisited: exploring hemoglobin and hemin scavengers as a novel class of therapeutic proteins, *Blood.* **121**, 1276-84.

53. Kassa, T., Jana, S., Meng, F. & Alayash, A. I. (2016) Differential heme release from various hemoglobin redox states and the upregulation of cellular heme oxygenase-1, *FEBS Open Bio.* **6**, 876-84.

54. Paoli, M., Anderson, B. F., Baker, H. M., Morgan, W. T., Smith, A. & Baker, E. N. (1999) Crystal structure of hemopexin reveals a novel high-affinity heme site formed between two beta-propeller domains, *Nat Struct Biol.* **6**, 926-31.

55. Hrkal, Z., Vodrazka, Z. & Kalousek, I. (1974) Transfer of heme from ferrihemoglobin and ferrihemoglobin isolated chains to hemopexin, *Eur J Biochem.* **43**, 73-8.

56. Camejo, G., Halberg, C., Manschik-Lundin, A., Hurt-Camejo, E., Rosengren, B., Olsson, H., Hansson, G. I., Forsberg, G. B. & Ylhen, B. (1998) Hemin binding and oxidation of lipoproteins in serum: mechanisms and effect on the interaction of LDL with human macrophages, *J Lipid Res.* **39**, 755-66.

57. Adams, P. A. & Berman, M. C. (1980) Kinetics and mechanism of the interaction between human serum albumin and monomeric haemin, *Biochem J.* **191**, 95-102.

58. Li, R. C., Saleem, S., Zhen, G., Cao, W., Zhuang, H., Lee, J., Smith, A., Altruda, F., Tolosano, E. & Dore, S. (2009) Heme-hemopexin complex attenuates neuronal cell death and stroke damage, *J Cereb Blood Flow Metab.* **29**, 953-64.

59. Larsen, R., Gouveia, Z., Soares, M. P. & Gozzelino, R. (2012) Heme cytotoxicity and the pathogenesis of immune-mediated inflammatory diseases, *Front Pharmacol.* **3**, 77.

60. Smith, A. & McCulloh, R. J. (2015) Hemopexin and haptoglobin: allies against heme toxicity from hemoglobin not contenders, *Front Physiol.* **6**, 187.

61. Meng, F. & Alayash, A. I. (2017) Determination of extinction coefficients of human hemoglobin in various redox states, *Anal Biochem.* **521**, 11-19.

62. Hanna, D. A., Harvey, R. M., Martinez-Guzman, O., Yuan, X., Chandrasekharan, B., Raju, G., Outten, F. W., Hamza, I. & Reddi, A. R. (2016) Heme dynamics and trafficking factors revealed by genetically encoded fluorescent heme sensors, *Proc Natl Acad Sci U S A.* **113**, 7539-44.

63. Ricoux, R., Sauriat-Dorizon, H., Girgenti, E., Blanchard, D. & Mahy, J. P. (2002) Hemoabzymes: towards new biocatalysts for selective oxidations, *J Immunol Methods.* **269**, 39-57.

64. Kawamura-Konishi, Y., Asano, A., Yamazaki, M., Tashiro, H. & Suzuki, H. (1998) Peroxidase activity of an antibody–ferric porphyrin complex, *Journal of Molecular Catalysis B: Enzymatic.* **4**, 181-190.

65. Cochran, A. G. & Schultz, P. G. (1990) Peroxidase activity of an antibody-heme complex, *Journal of the American Chemical Society.* **112**, 9414-9415.

66. Motterlini, R. & Otterbein, L. E. (2010) The therapeutic potential of carbon monoxide, *Nat Rev Drug Discov.* **9**, 728-43.

67. Rish, K. R., Swartzlander, R., Sadikot, T. N., Berridge, M. V. & Smith, A. (2007) Interaction of heme and heme-hemopexin with an extracellular oxidant system used to measure cell growth-associated plasma membrane electron transport, *Biochim Biophys Acta.* **1767**, 1107-17.

68. Miyamoto, Y., Nishimura, S., Inoue, K., Shimamoto, S., Yoshida, T., Fukuhara, A., Yamada, M., Urade, Y., Yagi, N., Ohkubo, T. & Inui, T. (2010) Structural analysis of lipocalin-type prostaglandin D synthase complexed with biliverdin by small-angle X-ray scattering and multi-dimensional NMR, *J Struct Biol.* **169**, 209-18.

69. Clarke, J. T. (1965) Purification and Analysis of Bilirubin, *Clin Chem.* **11**, 681-90.

70. Ishida, M., Dohmae, N., Shiro, Y. & Isogai, Y. (2003) Synthesis of biotinylated heme and its application to panning heme-binding proteins, *Anal Biochem.* **321**, 138-41.

71. Smith, G. P. (1985) Filamentous fusion phage: novel expression vectors that display cloned antigens on the virion surface, *Science.* **228**, 1315-7.

72. Smith, A. & Morgan, W. T. (1978) Transport of heme by hemopexin to the liver: evidence for receptor-mediated uptake, *Biochem Biophys Res Commun.* **84**, 151-7.

73. Eskew, J. D., Vanacore, R. M., Sung, L., Morales, P. J. & Smith, A. (1999) Cellular protection mechanisms against extracellular heme. heme-hemopexin, but not free heme, activates the N-terminal c-jun kinase, *J Biol Chem.* **274**, 638-48.

74. Smith, A., Rish, K. R., Lovelace, R., Hackney, J. F. & Helston, R. M. (2009) Role for copper in the cellular and regulatory effects of heme-hemopexin, *Biometals.* **22**, 421-37.

75. Kuross, S. A., Rank, B. H. & Hebbel, R. P. (1988) Excess heme in sickle erythrocyte inside-out membranes: possible role in thiol oxidation, *Blood.* **71**, 876-82.

76. Zhu, Y., Sun, Y., Jin, K. & Greenberg, D. A. (2002) Hemin induces neuroglobin expression in neural cells, *Blood.* **100**, 2494-8.

77. Mashima, R., Tilley, L., Siomos, M. A., Papalexis, V., Raftery, M. J. & Stocker, R. (2002) Plasmodium falciparum histidine-rich protein-2 (PfHRP2) modulates the redox activity of ferri-protoporphyrin IX (FePPIX): peroxidase-like activity of the PfHRP2-FePPIX complex, *J Biol Chem.* **277**, 14514-20.

78. Behrens, W. A. & Madere, R. (1987) A highly sensitive high-performance liquid chromatography method for the estimation of ascorbic and dehydroascorbic acid in tissues, biological fluids, and foods, *Anal Biochem.* **165**, 102-7.

Table 1: Summary of the sdAbs binding specificity against different tetrapyrroles.
SdAbs 1A6, 2H7 and 2H10 recognize (+) or not (-) the different tetrapyrroles and some only when at higher concentration (+/-).

	Tetrapyrroles									
sdAbs	**FePP**	**PP**	**GaPP**	**ZnPP**	**CoPP**	**SnPP**	**DeutPP**	**FePPCH3**	**BV**	**BR**
1A6	+	+	+	-	+	+	+	+	+/-	+/-
2H7	+	-	+	+	+	+	+	+/-	+/-	-
2H10	+	-	+	-	+	+	+	-	-	-

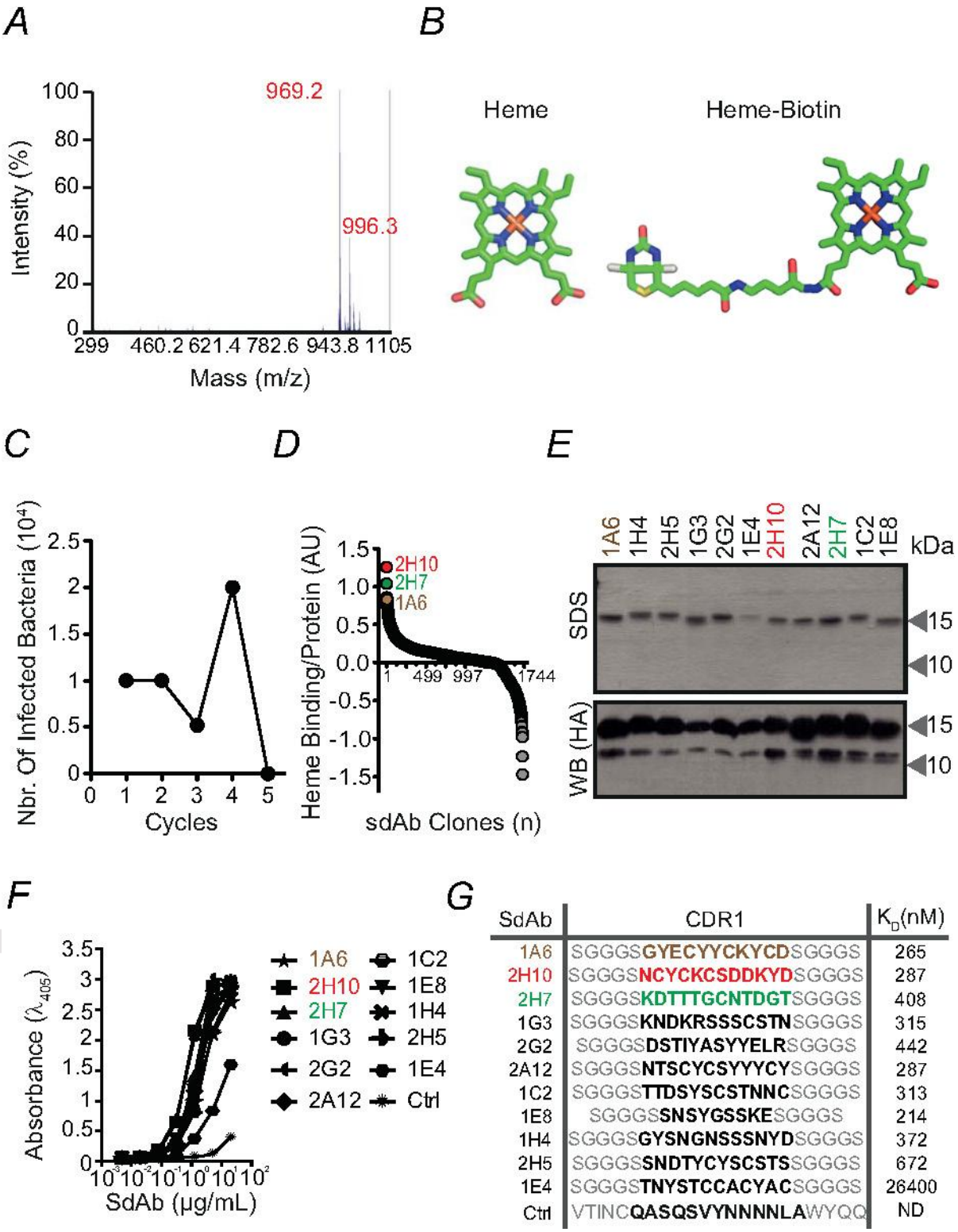

SdAb	CDR1	K_D(nM)
1A6	SGGGS**GYECYYCKYCD**SGGGS	265
2H10	SGGGS**NCYCKCSDDKYD**SGGGS	287
2H7	SGGGS**KDTTTGCNTDGT**SGGGS	408
1G3	SGGGS**KNDKRSSSCSTN**SGGGS	315
2G2	SGGGS**DSTIYASYYELR**SGGGS	442
2A12	SGGGS**NTSCYCSYYYCY**SGGGS	287
1C2	SGGGS**TTDSYSCSTNNC**SGGGS	313
1E8	SGGGS**SNSYGSSKE**SGGGS	214
1H4	SGGGS**GYSNGNSSSNYD**SGGGS	372
2H5	SGGGS**SNDTYCYSCSTS**SGGGS	672
1E4	SGGGS**TNYSTCCACYAC**SGGGS	26400
Ctrl	VTINC**QASQSVYNNNNLA**WYQQ	ND

FIGURE 1. Selection of heme-binding sdAbs using phage display technology. (*A*) MALDI-TOF/TOF analysis of biotinylated heme. Peak of mass-to-charge (m/z) 969.2 Da with characteristic isotopic cluster pattern, corresponding to biotinylation of a single hemin carboxylic acid residue. (*B*) Schematic representation (Accelrys draw 4.1 and 3D representations; Pymol software) of heme and biotinylated heme. (*C*) Elution cycles outputs of bacteria infected with phages displaying sdAbs recognizing heme. (*D*) Ratio of heme binding to protein expression of 1721 sdAb (circles) screened by ELISA, as described in *Experimental Procedures*. SdAbs 2H10, 2H7 and 1A6, with highest heme binding to protein expression ration, are highlighted. (*E*) SDS-PAGE of purified sdAbs stained by coomassie based stain or detected by western blot using an anti-HA mAb. (*F*) ELISA for recognition of solid-phase heme by purified sdAb. Ctrl: Control sdAb that does not recognize heme. (*G*) SdAb CDR1 aminoacid sequences, as determined by DNA sequencing. Binding affinity of SdAbs towards heme, determined by BIAcore surface Plasmon resonance.

Gouveia et al. Figure 2

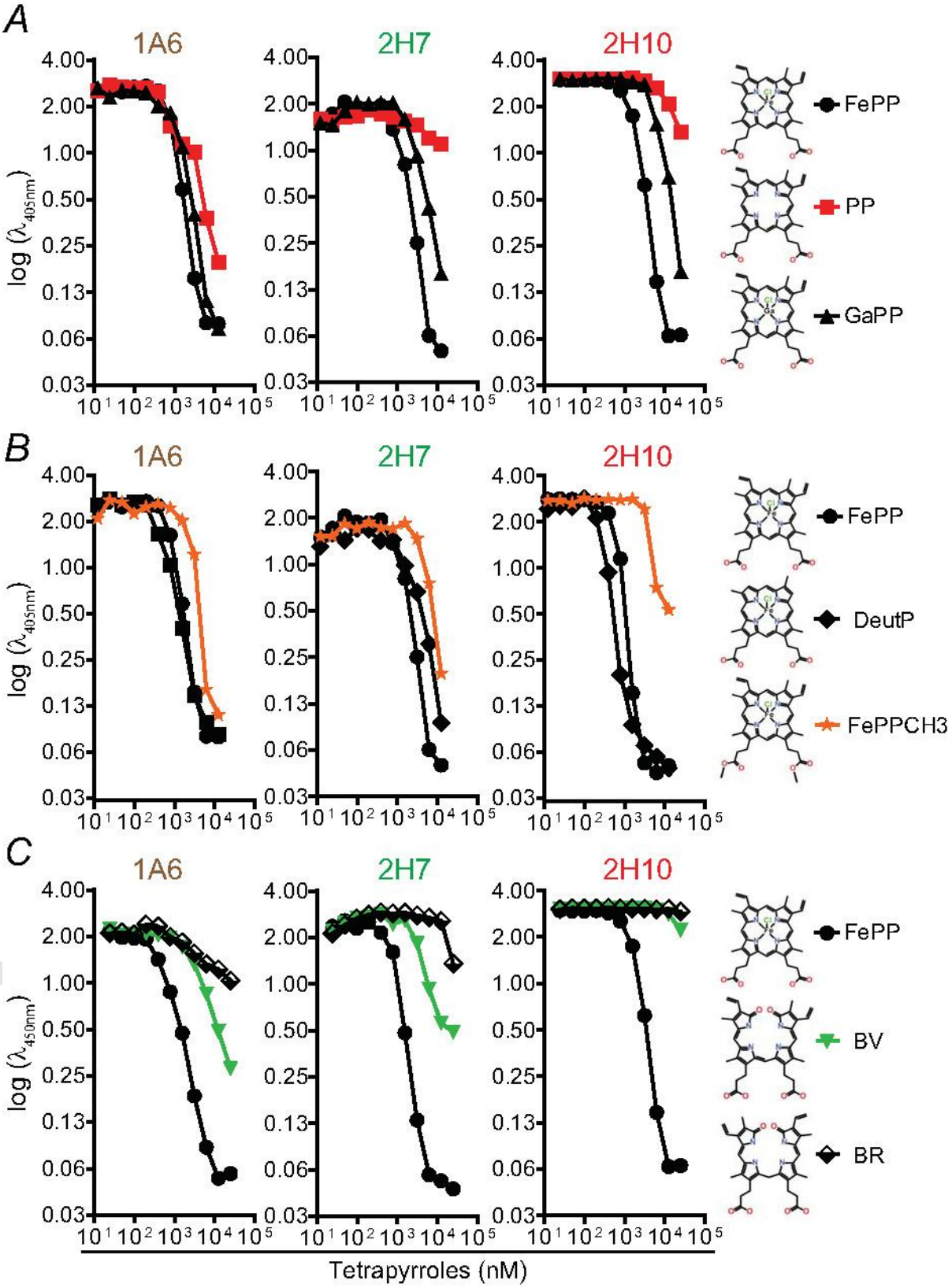

FIGURE 2. Assessment of sdAbs specificity against heme *vs.* related tetrapyrroles. Inhibitory effect of pre-incubation of sdAb with increasing concentrations of (*A*) FePP, PP or GaPP, (*B*) FePP, DeutP or FePPCH3, (*C*) biliverdin (BV) or bilirubin (BR) on sdAb binding to solid phase bound heme, measured by ELISA. Data from one out of three independent experiments with similar trend is shown.

Gouveia et al. Figure 3

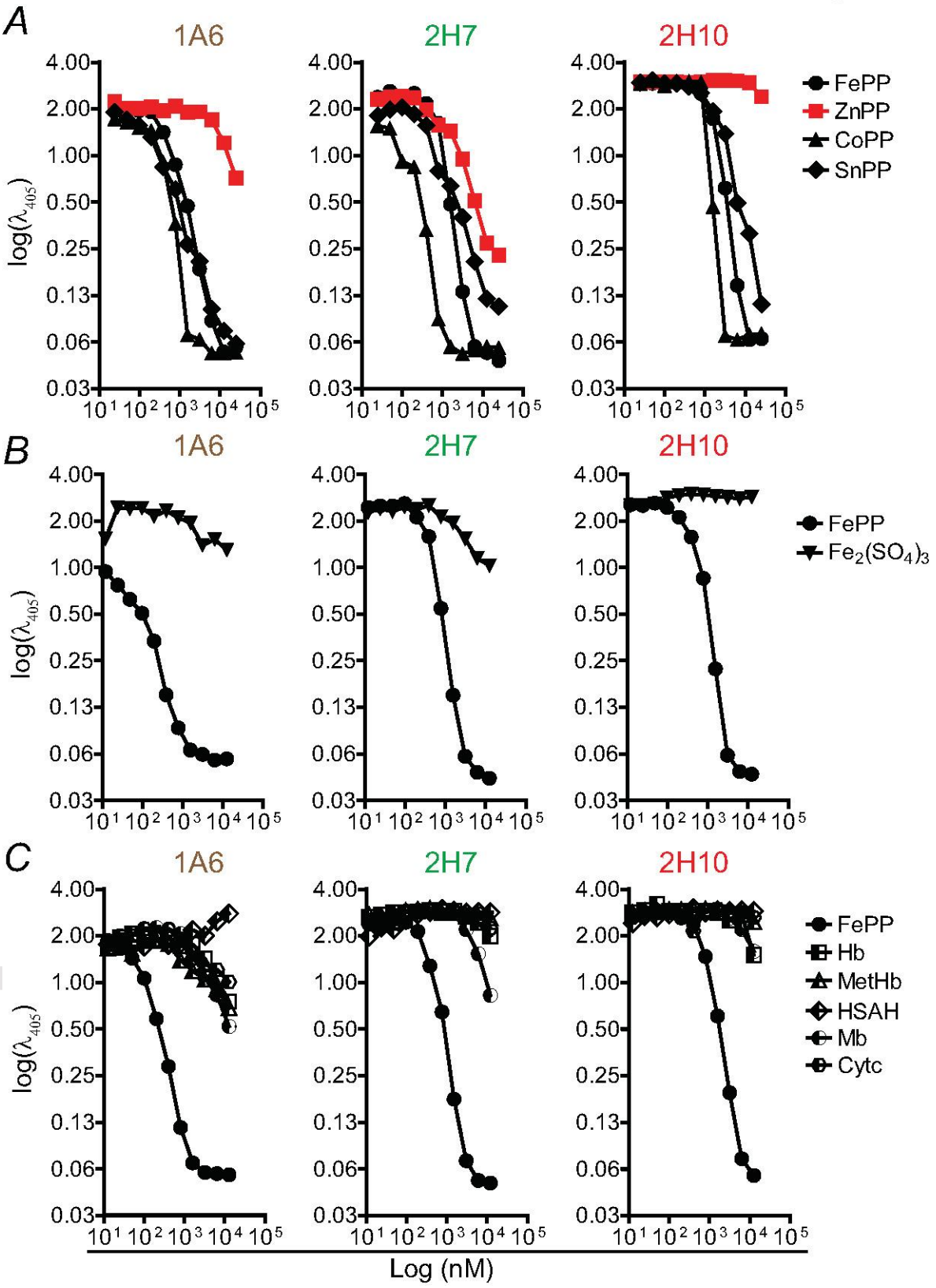

FIGURE 3. Assessment of sdAbs specificity against heme *vs.* heme analogs or heme contained in hemoproteins. Inhibitory effect of pre-incubation of sdAb with increasing concentrations of (*A*) FePP, ZnPP, CoPP or SnPP, (*B*) FePP or $Fe_2(SO_4)_3$ (*C*) FePP, Hb, oxidized Hb (MetHb), Myoglobin (Mb), Cytochrome c (Cytc) or human serum albumin bound to heme (HSAH), measured by ELISA. Data from one out of three independent experiments with similar trend is shown.

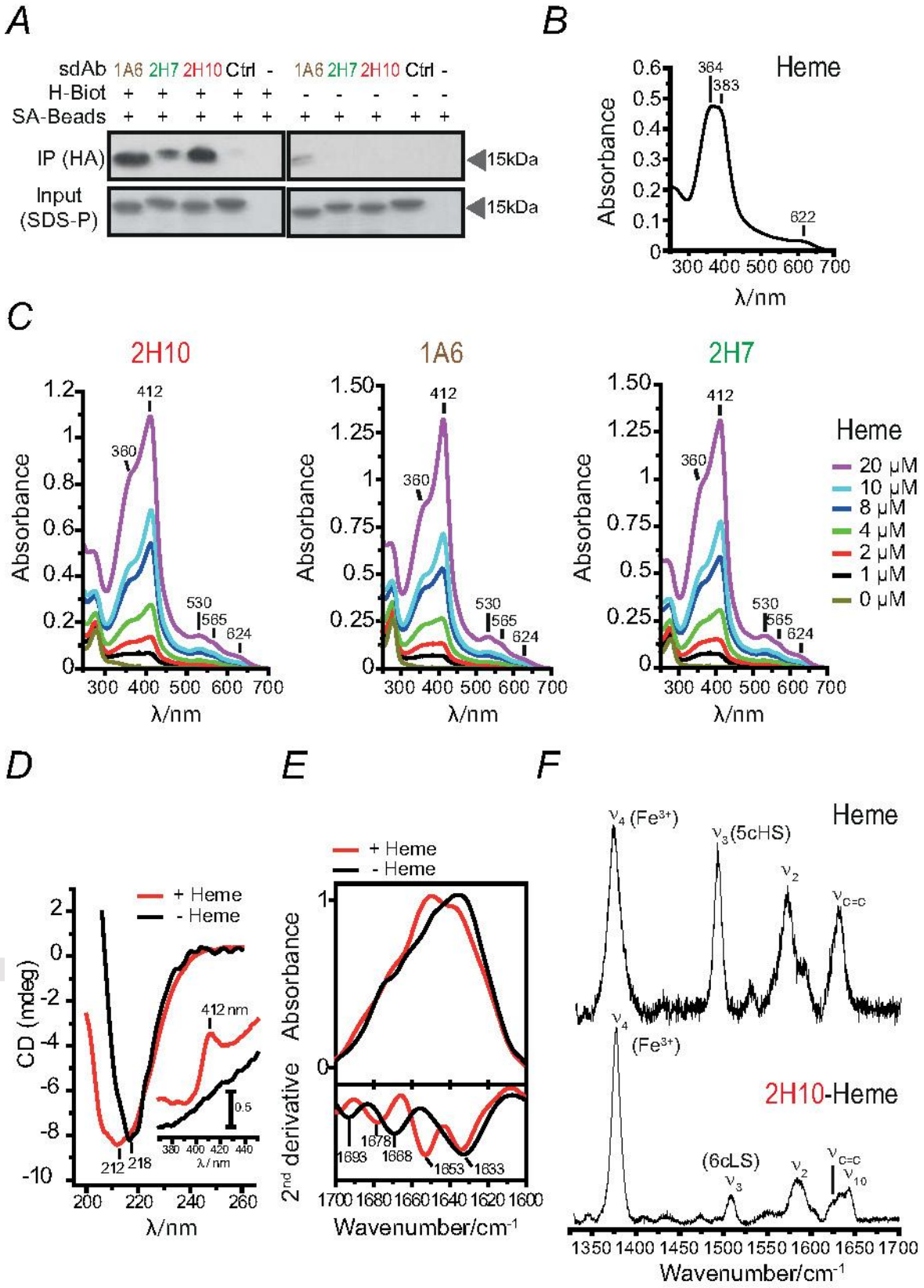

FIGURE 4. Analysis of heme binding by SdAbs. (*A*) SdAbs bound to biotinylated heme in solution were pooled-down using streptavidin (SA) beads and detected by western blot using anti-HA mAb. Input was measured by Coomassie-based stain. (*B*) UV-Visible spectra of hemin. Soret region at approximately 364 nm and 383 nm and a CT band at 622 nm are shown, representative of three independent experiments. (*C*) UV-visible spectra of sdAb 2H10, 1A6 and 2H7 bound to heme at different concentrations. Soret (412 nm), Q_1 (530 nm), Q_0 (565 nm) and CT (624 nm) bands are highlighted. (*D*) Far UV CD spectra of sdAb 2H10 in the apo (black) and heme-bound (red) forms. Shift from 212 to 218 is due to heme-driven conformational rearrangement of the sdAb secondary structure. The inset shows the Soret region, with the appearance of the 412 nm band, due to heme binding to the sdAb. (*E*) ATR FTIR absorption spectra (top) and second derivative (bottom) of sdAb 2H10 in the apo (black) and heme-bound (red) forms in the amide I region (1700-1610 cm^{-1}), showing structural modification upon heme coordination. (*F*) High frequency Resonance Raman spectra of hemin and sdAb 2H10 bound to hemin, obtained with 413 nm excitation.

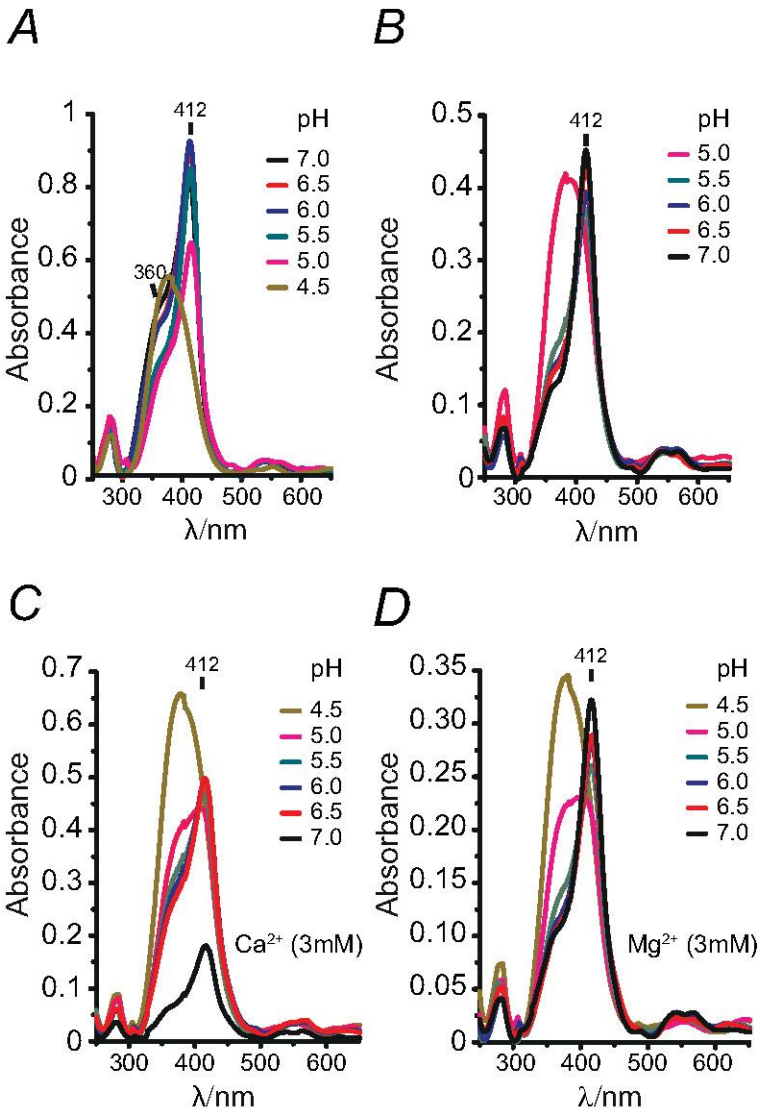

FIGURE 5. Effect of the pH and divalent cations on heme binding by sdAb. (*A*) UV-visible spectra of heme binding by sdAb 2H10 bound under gradual pH decrease by the addition of HCl. (*B*) UV-visible spectra of sdAb 2H10 bound to heme under gradual pH neutralization by the addition of KOH. (*C*) UV-visible spectra of sdAb 2H10 bound to heme under gradual pH neutralization by the addition of KOH in the presence of calcium (Ca^{2+}; 3mM) or (*D*) magnesium (Mg^{2+}; 3mM). The divalent cations Ca^{2+} impair the binding of the sdAb to heme contrarily to the magnesium (Mg^{2+}). Data is representative of three independent experiments with similar trend.

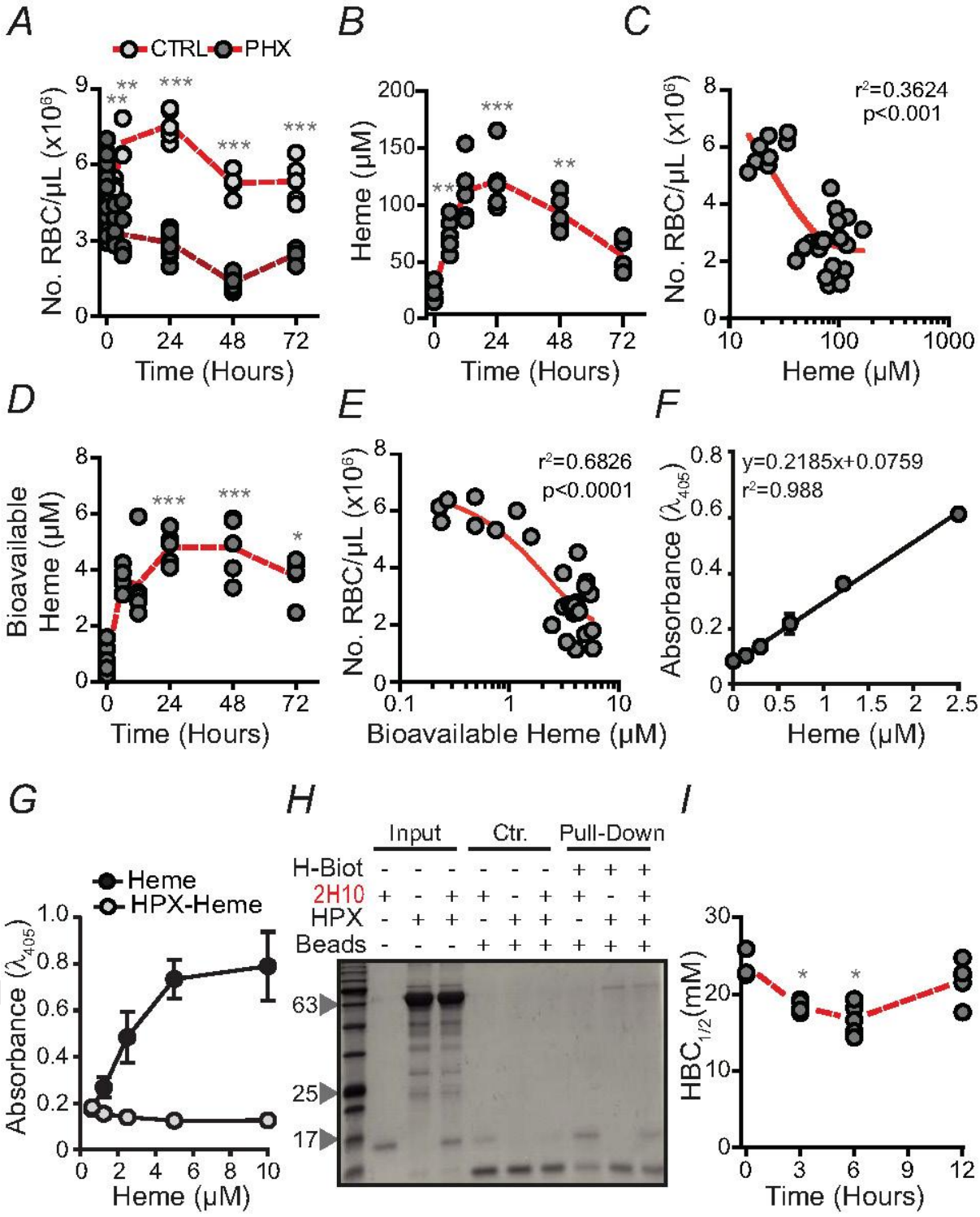

FIGURE 6. Characterization of labile heme in plasma following acute hemolysis. (*A*) Number of RBC in C57BL/6 mice receiving Phenylhydrazine (PHX) and control (CTRL) mice receiving PBS. (*B*) Heme concentration in the plasma of C57BL/6 mice receiving phenylhydrazine. (*C*) Correlation between circulating RBC numbers (data from A) and heme concentration in plasma (data from B) in C57BL/6 mice receiving phenylhydrazine. (*D*) Concentration of bioavailable heme in plasma of C57BL/6 mice receiving phenylhydrazine, quantified by a heme reporter assay [31]. (*E*) Correlation between circulating RBC numbers (data from A) and concentration of bioavailable heme in plasma (data from *D*) in C57BL/6 mice receiving phenylhydrazine. (F) Soluble hemin quantified by a sandwich ELISA in which the sdAbs 1A6 and 2H7 are used to capture and reveal heme, respectively. (*G*) Detection of soluble heme *vs.* heme bound to HPX using the same sdAb-based ELISA as in (F). The sdAb-sandwich based ELISA was used to verify whether the sdAbs can recognize heme bound to HPX. This assay reveals that heme bound to HPX is not detected by the sdAbs. (*H*) A pull-down assay using streptavidin-beads and heme-biotin was used to demonstrate that heme-biotin bound to sdAb 2H10 can be removed by HPX. To the 2H10 SdAb bound to heme-biotin was added HPX (1/6 SdAb/HPX molar ratio) and then heme biotin bound protein was pulled-down using streptavidin-beads. Streptavidin-beads pulled-down the sdAb 2H10 as well as HPX bound to heme-biotin, demonstrating once more the ability of HPX to bind to heme-bound to sdAb 2H10. The data obtained in both assay is consistent with the higher affinity of HPX towards heme as compared to the sdAb 2H10. Coomassie-based stain of 15% SDS-PAGE gel loaded with streptavidin-beads used to pull-down heme-biotin from different reaction mixtures composed of 2H10 sdAb and/or HPX and/or heme-biotin. Grey arrowheads indicate the molecular weight of the protein ladder (NZYColour Protein Marker II, Nzytech ®) in kDa loaded in the first lane of the gel. Gel is representative of two independent experiments with similar trend. (*I*) Plasma $HBC_{1/2}$ in C57BL/6 mice receiving phenylhydrazine. Circles in A, B, C, D, E and I correspond to individual mice. Each circle corresponds to an individual mouse. Red dash line represents mean ± STD. *p<0.05, ** p<0.01, ***p<0.001 versus time 0, calculated by ANOVA and Dunns post-test.

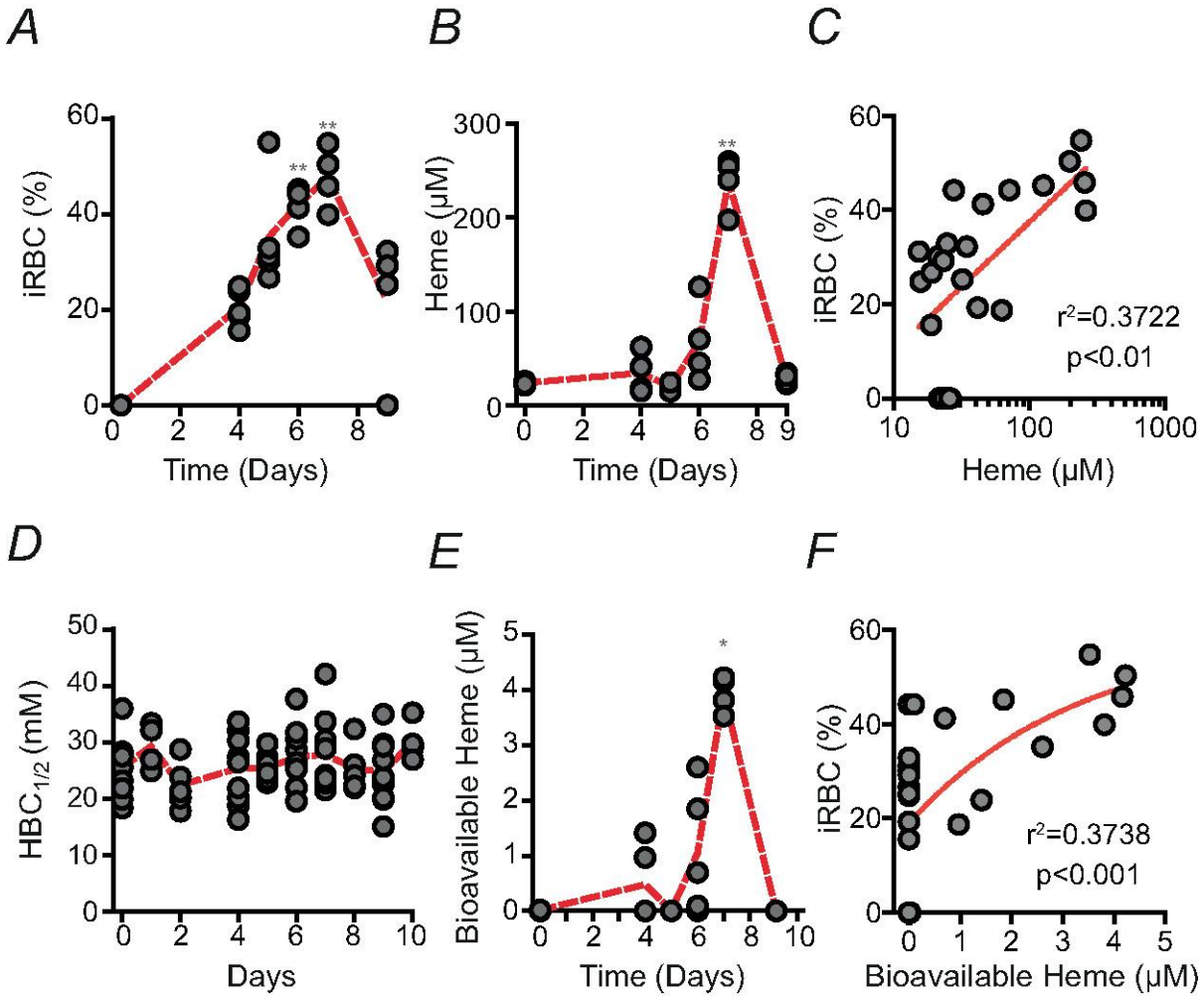

FIGURE 7. Characterization of labile heme in plasma following *Plasmodium* infection. (*A*) Percentage of infected RBC (iRBC) and (*B*) heme concentration in plasma of C57BL/6 mice (n=4-5) infected with *Pcc* . (*C*) Correlation between percentage of iRBC (data from A) and heme concentration in plasma (data from B). (*D*) $HBC_{1/2}$ in *Pcc* infected C57BL/6 mice. (*E*) Bioavailable heme in *Pcc* infected C57BL/6 mice. (*F*) Correlation between the percentage of iRBC (data from *A*) and bioavailable heme (data from *E*). *p<0.05 and ** p<0.01 versus time 0, established by ANOVA and Dunns post-test. Circles correspond to individual mice. Red dash line represents mean from mice pooled from 2-3 independent experiments with similar trend.

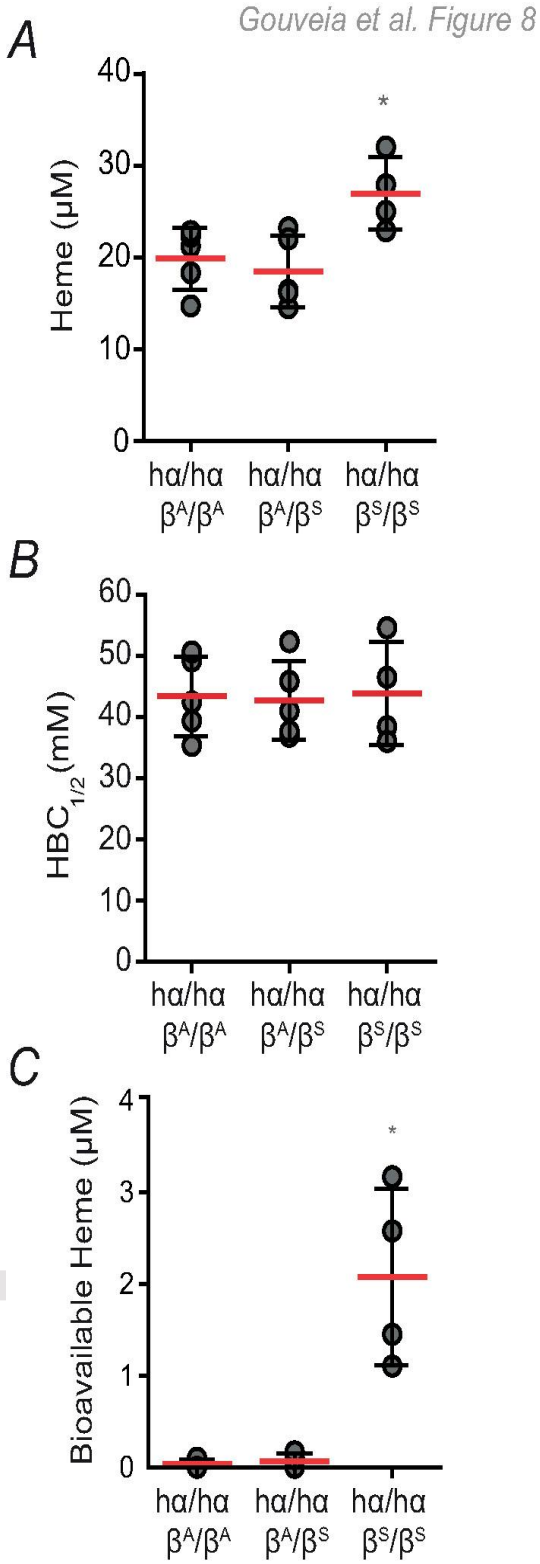

FIGURE 8. Heme accumulation in plasma in sickle-cell disease. (*A*) Total heme, (*B*) $HBC_{1/2}$ and (*C*) bioavailable heme in sickle hα/hα::β^S/β^S versus control hα/hα::β^A/β^A and hα/hα::β^A/β^S mice. *$p < 0.05$ established by ANOVA and Dunns post-test. Each circle corresponds to an individual mouse. Red dash line represents mean ± STD.

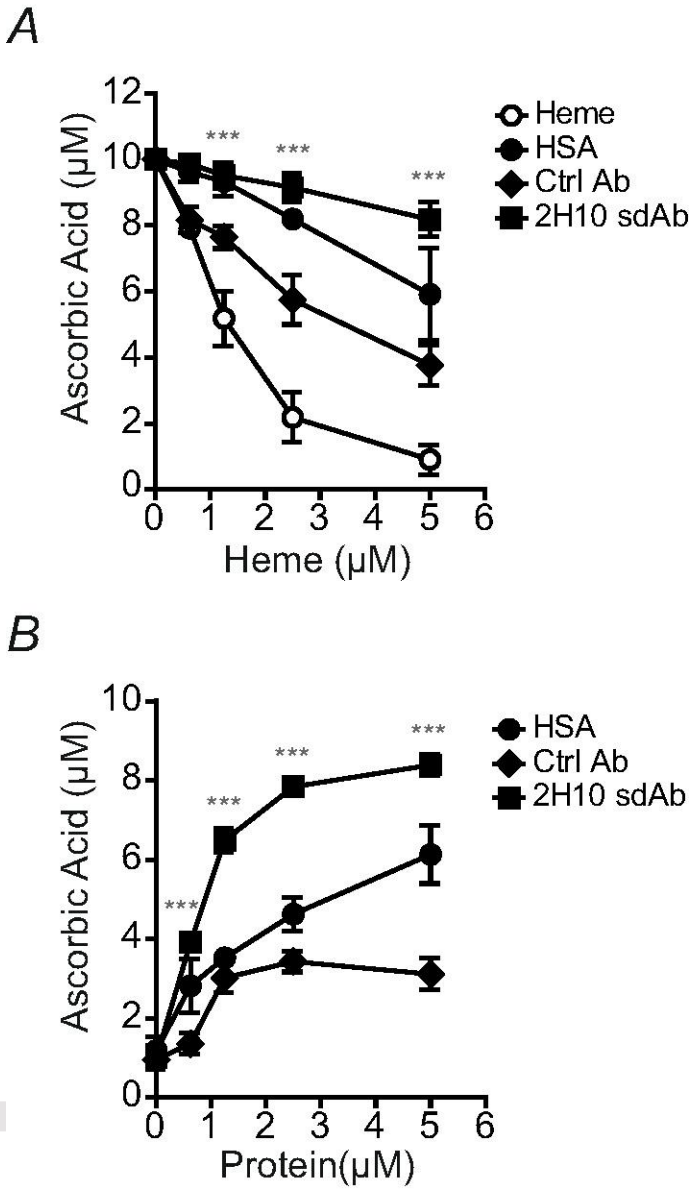

FIGURE 9. Targeting heme with sdAbs. Ascorbate oxidation by heme in the presence or absence of sdAb 2H10, control (Ctrl) sdAb or human serum albumin (HSA) under (*A*) increasing heme or (*B*) protein concentrations. Results shown are the mean ± SEM from four (*A*) and three (*B*) independent experiments. *** Mean value of sdAb 2H10 differs from the corresponding mean point value of Ctrl sdAb at the $p < 0.001$.

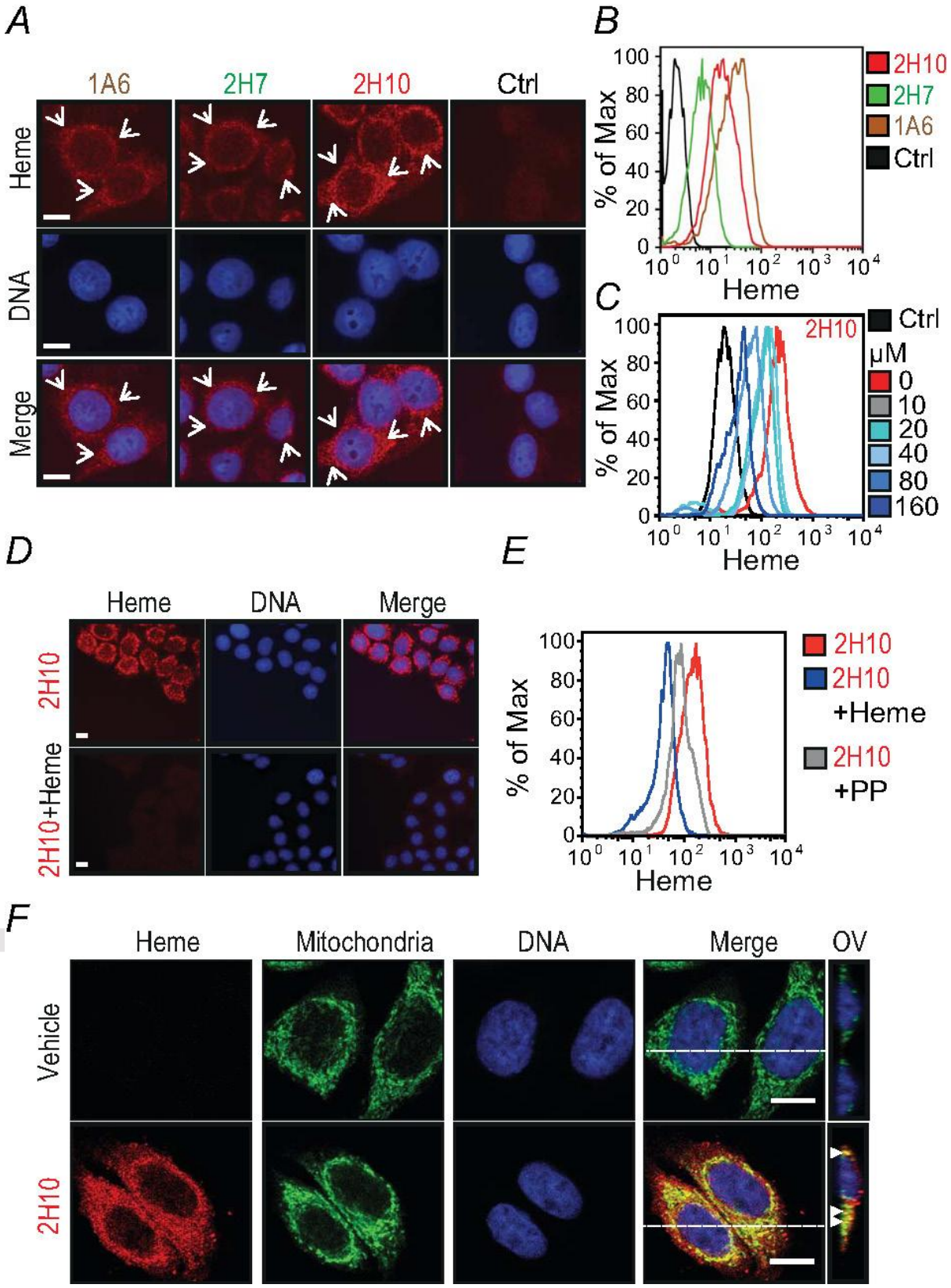

FIGURE 10. Detection of intracellular heme using sdAbs. (*A*) Intracellular heme (red) and DNA (blue) in HeLa cells, detected by immunoflurescence using different heme-specific sdAbs and DAPI, respectively. Staining with a control sdAb (Ctrl) that does not recognize heme, is shown. Scale bar, 10 μM. Arrows highlight heme staining. (*B*) Detection of intracellular heme by flow cytometry in HeLa cells, using the same sdAbs as in (*A*). (*C*) Same as (*B*), with pre-incubation of sdAb 2H10 with increasing concentrations (0-160 μM) of hemin in solution. (*D*) Same as (A), using sdAb 2H10 pre-incubated or not with hemin (160 μM) in solution. (*E*) Same as (*C*), with sdAb 2H10 pre-incubated with heme (160 μM) or PP (160 μM). (*F*) Same as (*A*), in HeLa cells co-stained with MitoTracker® for mitochondria localization (Green). Heme was detected using the sdAb 2H10 (red) and DNA with DAPI (blue). Merged images show co-localization of heme with mitochondria (yellow). For each condition Z-stacks were acquired and orthogonal view (OV) of the dashed line is shown. Arrows highlight co-localization. All images with a scale bar, 10 μm. Data in *A-D* are representative of three independent experiments with similar trend.

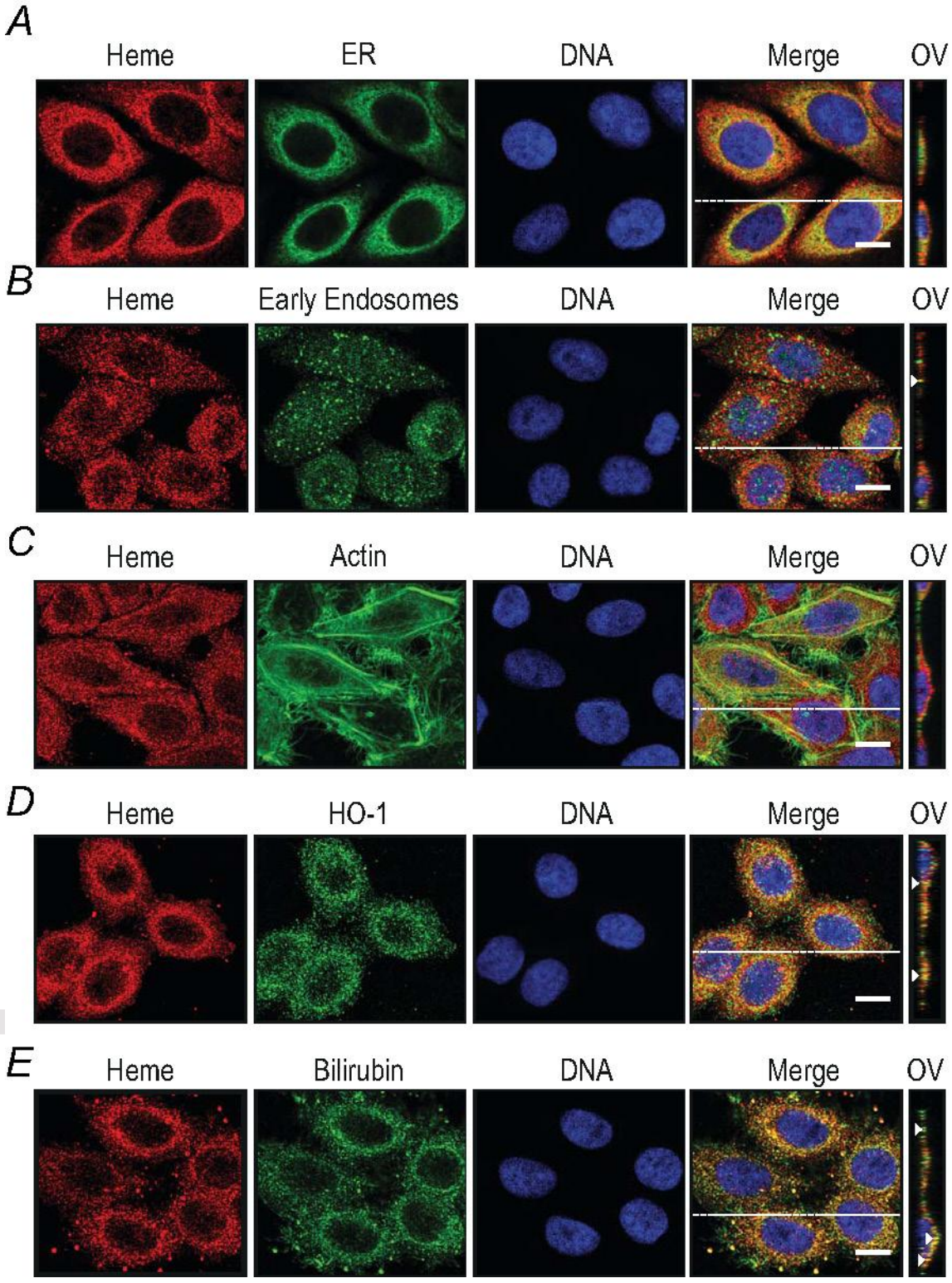

FIGURE 11. Detection of intracellular heme using sdAbs. Heme (red) and DNA (blue) detected by immunofluorescence in HeLa cells using the sdAb 2H10 and DAPI, respectively. Cells were co-stained (green) with (*A*) anti-Calnexin for endoplasmatic reticulum (ER) (*B*) anti-EEA-1 for endosomes, (*C*) a phalloidin–tetramethylrhodamine B isothiocyanate for F-actin, (*D*) anti-HO-1 polyclonal Ab and (*E*) anti-bilirubin mAb. Merged figures show co-localizations (yellow). For each condition Z-stacks were acquired and orthogonal view (OV) of the dashed line is shown. Arrows highlight co-localization. Data shown is representative of three independent experiments with similar results. All images with a scale bar, 10 μm.